EXPLORING THE MOLECULAR INTERACTIONS BETWEEN HOST CELLS AND *Cryptosporidium parvum* DURING INVASION

A Dissertation

by

XUE YU

Submitted to the Office of Graduate and Professional Studies of
Texas A&M University
in partial fulfillment of the requirements for the degree of

DOCTOR OF PHILOSOPHY

Chair of Committee,	Guan Zhu
Committee Members,	Michael Criscitiello
	Gregory Johnson
	Yanan Tian
Head of Department,	Ramesh Vemulapalli

August 2018

Major Subject: Veterinary Pathobiology

ABSTRACT

Cryptosporidium parvum is a zoonotic protozoan parasite belonging to the Phylum Apicomplexa and a causative agent of mild to severe watery diarrhea in humans and animals. The infection starts with the ingestion of oocysts, often from contaminated water, followed by the release of four sporozoites from individual oocysts in the small intestine and the invasion of sporozoites into intestinal epithelial cells. A unique, host cell-derived parasitophorous vacuole membrane (PVM) will be formed during the parasite invasion to contain the intracellular developing parasites. However, the essential molecular interactions between the parasite and host cells during infection and the mechanism of PVM formation are poorly understood.

The study employed two approaches to study the molecular mechanisms of invasion by the *C. parvum* sporozoites. The first approach focused on identifying host cell factors, in which three host cell mutants generated with UV-irradiation-based mutagenesis have significantly increased resistance to the invasion by *C. parvum* sporozoites. One of the mutants was significantly resistant to the attachment of sporozoites onto host cells, and can be used to identify genes and pathways responsible for the parasite attachment by forward genetics. The second approach focused on a multifunctional parasite protein, which is discharged to the host cell surface during the parasite invasion. There was strong evidence indicating that this parasite protein participated in the aggregation of host cell filamentous actin (F-actin) and was associated with the formation of PVM.

This study has not only generated new knowledge towards understanding the mechanisms of *C. parvum* infection, but also identified new directions to further explore the molecular pathways in the host cells and the parasites responsible for the parasite invasion.

DEDICATION

To my curiosity, which keeps me trying new things, exploring the unknown and discovering myself.

ACKNOWLEDGEMENTS

I would like to thank my committee chair, Dr. Guan Zhu, for his guidance in my research career. I want to thank my committee members, Dr. Criscitiello, Dr. Johnson and Dr. Tian, for their guidance and support throughout the course of this research. I also want to thank Dr. Cai for teaching and guiding me in the study of bioinformatics.

Thanks go to all my lab members, friends, colleagues, department faculty, and staff for making my time at Texas A&M University a great experience. Thanks also go to Rachel Hoyle for making my life in the United States colorful, and to Chris Hill for helping me at the beginning of my life in the United States.

Finally, thanks to my husband for his support, patience and love and thanks to my son for giving me a great experience as a mother.

CONTRIBUTORS AND FUNDING SOURCES

This work was supervised by a dissertation committee consisting of Professor Guan Zhu and Professor Michael Criscitiello from the Department of Veterinary Pathobiology, Professor Gregory Johnson from the Department of Veterinary Integrative Biosciences, and Professor Yanan Tian from the Department of Veterinary Physiology and Pharmacology. All work for this dissertation was completed independently by the student.

The study was supported in part by grants from the National Institute of Allergy and Infectious Diseases (NIAID) and National Institutes of Health (NIH) (R21 AI136663 and R21 AI103668).

NOMENCLATURE

aa-tRNA	Aminoacyl-tRNA
AIDS	Acquired immunodeficiency syndrome
BSA	Bovine serum albumin
C	Cycle number
Ca^{2+}	Calcium ions
CCD	Charge-coupled device
CDC42	Cell division control protein 42
cDNA	Complementary DNA
CO_2	Carbon dioxide
COWPs	*Cryptosporidium* oocyst wall proteins
Cp	*Cryptosporidium parvum*
CpEF1α	*Cryptosporidium parvum* elongation factor 1α
CpEF1β	*Cryptosporidium parvum* elongation factor 1β
CpEF1γ	*Cryptosporidium parvum* elongation factor 1γ
CpERF3	*Cryptosporidium parvum* eukaryotic peptide chain release factor 3
CpLDH	*Cryptosporidium parvum* lactate dehydrogenase
CpTMPs	*Cryptosporidium parvum* total membrane proteins
CSL	Circumsporozoite-like
DAPI	4’,6-diamidino-2-phenylindole
DIC	Differential interference microscopy
DNAase	Deoxyribonuclease

ECL	Enhanced chemiluminescence
ED	Electron-dense
eEF1α	Eukaryotic elongation factor 1α
EF-Tu	Elongation factor thermo untable
F_0	Fluorescent units at cycle zero
F_b	Background RFU
FBS	Fetal bovine serum
F_c	RFU at cycle *C*
FDA	Food and Drug Administration
FITC	Fluorescein isothiocyanate
F_{max}	Maximal RFU
FO	Feeder organelle
Gal/GalNAc	Galactose-N-acetylgalactosamine
GDP	Guanosine-5'-diphosphate
GFP	Green fluorescent protein
GP	Glycoprotein
GPI	Glycosylphosphatidylinositol
GTP	Guanosine-5'-triphosphate
h	Hour
HCT-8	Human ileocecal colorectal adenocarcinoma cell line
HIV	Human Immunodeficiency Virus
HR	High resolution
HSF	Heat shock factor

IgG	Immunoglobulin G
ITGA2	Integrin α2
MBP	Maltose-binding protein
N-WASP	Neural Wiskott-Alrich syndrome protein
NCBI	National Center for Biotechnology Information
NDD	Non-Descanned Detector
NTZ	Nitazoxanide
ORF	Open-reading frame
PBS	Phosphate-buffered saline
PCR	Polymerase chain reaction
pH	potential of hydrogen
PI	Isoelectric point
PI3K	Phosphatidylinositol-3-kinase
PV	Parasitophorous Vacuole
PVM	Parasitophorous Vacuole Membrane
qRT-PCR	Quantitative reverse transcription polymerase chain reaction
RAP	Arginine aminopeptidase
RdRP	RNA-dependent RNA polymerase
RFU	Relative fluorescent unit
RNA	Ribonucleic acid
RNAase	Ribonuclease
RPM	Revolutions per minute
RPMI-1640	Roswell Park Memorial Institute medium

rRNA	Ribosomal ribonucleic acid
RT-PCR	Reverse transcription polymerase chain reaction
SDS-PAGE	Sodium dodecyl sulfate polyacrylamide gel electrophoresis
SPF	Specific pathogen-free
TEV	Tobacco etch virus
TRAPs	Thrombospondin-related adhesive proteins
TRITC	Tetramethylrhodamine isothiocyanate
UV	Ultraviolet
UV-B	Ultraviolet B
VASP	Vasodilator-stimulated phosphoprotein
WT	Wild-type

TABLE OF CONTENTS

Page

LIST OF FIGURES

Page

LIST OF TABLES

Page

CHAPTER I

INTRODUCTION AND LITERATURE REVIEW

1.1 History of *Cryptosporidium spp*. and cryptosporidiosis

More than 110 years ago, *Cryptosporidium* species were first described in the gastric glands of an asymptomatic laboratory mouse by Ernest E. Tyzzer (Tyzzer 1907). The morphology of *Cryptosporidium muris* and *Cryptosporidium parvum* in different life stages were then described in 1910 and 1912 respectively (Tyzzer 1910, Tyzzer 1912). After discovering *Cryptosporidium*, the protozoan was thought to be a benign commensal organism and was neglected for more than half a century. It was not until the 1970s that *Cryptosporidium* infection was discovered extensively in the gastrointestinal or respiratory tract of most animal species, including mammals, reptiles and birds, causing them watery diarrhea termed as cryptosporidiosis (Ramirez et al. 2004, Richter et al. 2011, Nakamura and Meireles 2015). In April of 1976, using light and electron microscopic detection in a rectal biopsy, *Cryptosporidium* infection in a human being was reported: a 3-year-old child with severe acute enterocolitis. The infection caused pathological changes in her rectum and severe clinical symptoms, suggesting the pathogenicity of the *Cryptosporidium* infection (Nime et al. 1976). During June of the same year, another case was reported: a 39-year-old man who developed overwhelming diarrhea after taking immunosuppressed drugs daily for 5 weeks. Severe mucosal injury and epithelial surface infection with tiny organisms found in Jejunal and ileal biopsies. After discontinuation of immunosuppressed drugs for 2 weeks, the diarrhea was resolved with the clearance of *Cryptosporidium* infection (Meisel et al. 1976). Thus, cryptosporidiosis is an opportunistic infection causing severe watery diarrhea of immunosuppressed patients. Between 1980 and

1983, a series of scientific papers published on cross-transmission experiments using *Cryptosporidium* from different animal species and humans suggest that mammalian *Cryptosporidium* lacks host specificity. However, it is only partially true. *Cryptosporidium hominis*, which is specific to the human species, was discovered 20 years later (Morgan-Ryan et al. 2002). The transmission experiments were the first in vivo studies of laboratory rodents and made the screening of anti-Cryptosporidial drugs possible (Tzipori et al. 1982).

Cryptosporidiosis was brought to public attention in the early 1980s because of its strong association with the death of immunocompromised people, especially HIV/AID patients (Ma and Soave 1983, Ma 1984). Cryptosporidiosis is an opportunistic infection causing weight loss, severe dehydration and malnutrition in HIV positive patients, which can be fatal. Thanks to the discovery and extensive use of anti-retroviral therapy between 1997 and 2007, the rate of cryptosporidiosis infection among HIV/AIDS patients has gone down considerably in developed countries. However, cryptosporidiosis remains a relevant problem and causes severe dehydration and malnutrition today for immunocompromised people, especially HIV/AIDS patients, and children under 2 years old in developing countries (Tumwine et al. 2005, Checkley et al. 2015).

The transmission and outbreaks of cryptosporidiosis due to contaminated water were not brought to public attention until several notable outbreaks in the late 1970s and early1980s. In 1978, a waterborne outbreak of cryptosporidiosis in Carrollton, Georgia, United States of America (USA) affected about 13,000 people (Hayes et al. 1989). In 1980, a cryptosporidiosis outbreak occurred in Swindon and Oxfordshire in England affecting about 5,000 people. The largest cryptosporidiosis outbreak occurred in Milwaukee, Wisconsin, USA in 1993, where 400,000 people were affected. The magnitude of this outbreak brought to public and government attention the fact that drinking contaminated water is a source and major risk factor for a

cryptosporidiosis outbreak (Mac Kenzie et al. 1994). In the following decades, a large number of experiments were conducted on *Cryptosporidium*, which expanded our knowledge of these parasites extensively. The genome of *C. parvum* and *C. hominis* were sequenced in 2004, which further advanced our knowledge on these parasites (Abrahamsen et al. 2004, Xu et al. 2004). However, despite these advancements, there is only one FDA approved drug, Nitazoxanide (NTZ), to treat cryptosporidiosis in immunocompetent people in the United States (Abrahamsen et al. 2004, Xu et al. 2004, Rossignol et al. 2001). For immunocompromised people, like HIV/AIDS patients and children under 3 years old, no effective drugs are available (Amadi et al. 2002).

Based on clinical and epidemiological studies, cryptosporidiosis was responsible for the outbreak of neonatal diarrhea in economical important animals including calves and lambs (Tzipori et al. 1980, Tzipori et al. 1983). Despite the economic loss caused by cryptosporidiosis in farm animals, no approved effective treatment is currently available (Shahiduzzaman and Daugschies 2012). There are several published drug therapies of *Cryptosporidium* infection in animals, for example azithromycin, nitazoxanide, and paromomycin. Azithromycin, which is a macrolide antibiotic, showed the ability to suppress oocyst shedding in infected calves, but there have been no sufficient clinical trials to prove its suitability in treating cryptosporidiosis in animals ((Elitok et al. 2005, Shahiduzzaman and Daugschies 2012). Nitazoxanide (NTZ), which is a FDA-approved drug to treat human cryptosporidiosis, showed various effects on animals (Abubakar et al. 2007, Ollivett et al. 2009, Schnyder et al. 2009). Paromomycin, an aminoglycoside antibiotic, showed limited efficacy against cryptosporidiosis in piglets and goats, but cannot be used on large ruminants (Marshall and Flanigan 1992, Theodos et al. 1998, Johnson et al. 2000, Shahiduzzaman and Daugschies 2012).

1.2 Life cycle of *Cryptosporidium spp.*

Cryptosporidium parasites have a direct life cycle (**Figure 1.1**). As seen in the figure, after oocysts excystate in the lumen of host intestines (a), sporozoites (b) attach onto host cells and develop into trophozoites (c) within parasitophorous vacuoles membranes (PVM) and are confined to the microvillus region of the mucosal epithelium. Trophozoites go through asexual division (merogony) (d and e) to form merozoites, which are released from type I meronts. The merozoites will invade host cells to again form either type I meronts (e), or to form type II meronts (f). Type II meronts form the sexual stages, microgamonts (g) and macrogamonts (h). About 80% of zygotes (i) formed from the fertilization of the macrogametes by the microgametes develop into thick-walled oocysts and are excreted into environment forming sporulated oocysts (j) and contain four sporozoites. Sporulated oocysts transmit the infection from one host to another and can survive through chlorine at concentrations used for water treatment. About 20% of zygotes form single layer thin-walled oocysts (k) and cause auto-infection that can maintain the parasite in the host without repeated ingestion of the thick-walled oocysts from the environment. Each oocyst (thin and thick-walled) ranges in size from 3.7 to 8.4 μm in length and 3.2 to 6.3 μm in width, and contains four sporozoites. When oocysts are ingested via the fecal-oral route, such as drinking contaminated water, by a human or animal host, sporozoites will be released from the oocysts and invade intestinal epithelial cells. During the invasion, a sporozoite (zoite) attaches onto the host cell surface, where the host cell membrane forms a fold to encircle the apical end of the zoite. The membrane fold/rim gradually rises up along the surface of zoite and fuses together to fully cover the zoite (Valigurova et al. 2008). The host cell derived membrane is termed parasitophorous vacuole (PV) membrane (PVM). The sporozoite will undergo a morphological change to become a nearly round

trophozoite during the invasion process, starting its intracellular, but extra cytoplasmic development. The trophozoite in the PV will first undergo asexual development (aka merogony) to form type I meronts containing 8 or 16 merozoites that will be released to infect neighbor host cells. After at least two rounds of merogony, the parasite will form type II meronts containing four merozoites and invade new host cells, entering sexual development (aka gametogenesis) to form microgametes and macrogametes. A macrogamete is fertilized by a microgamete, forming a zygote. Zygotes will further develop into oocysts containing four sporozoites. The oocysts consist of 80% two-layer thick wall oocysts, which will be excreted into the environment to start a new life cycle upon ingestion by a new host, and 20% one-layer thin wall oocysts, which cause auto-infection and leads to persistent and chronic infection (Bouzid et al. 2013).

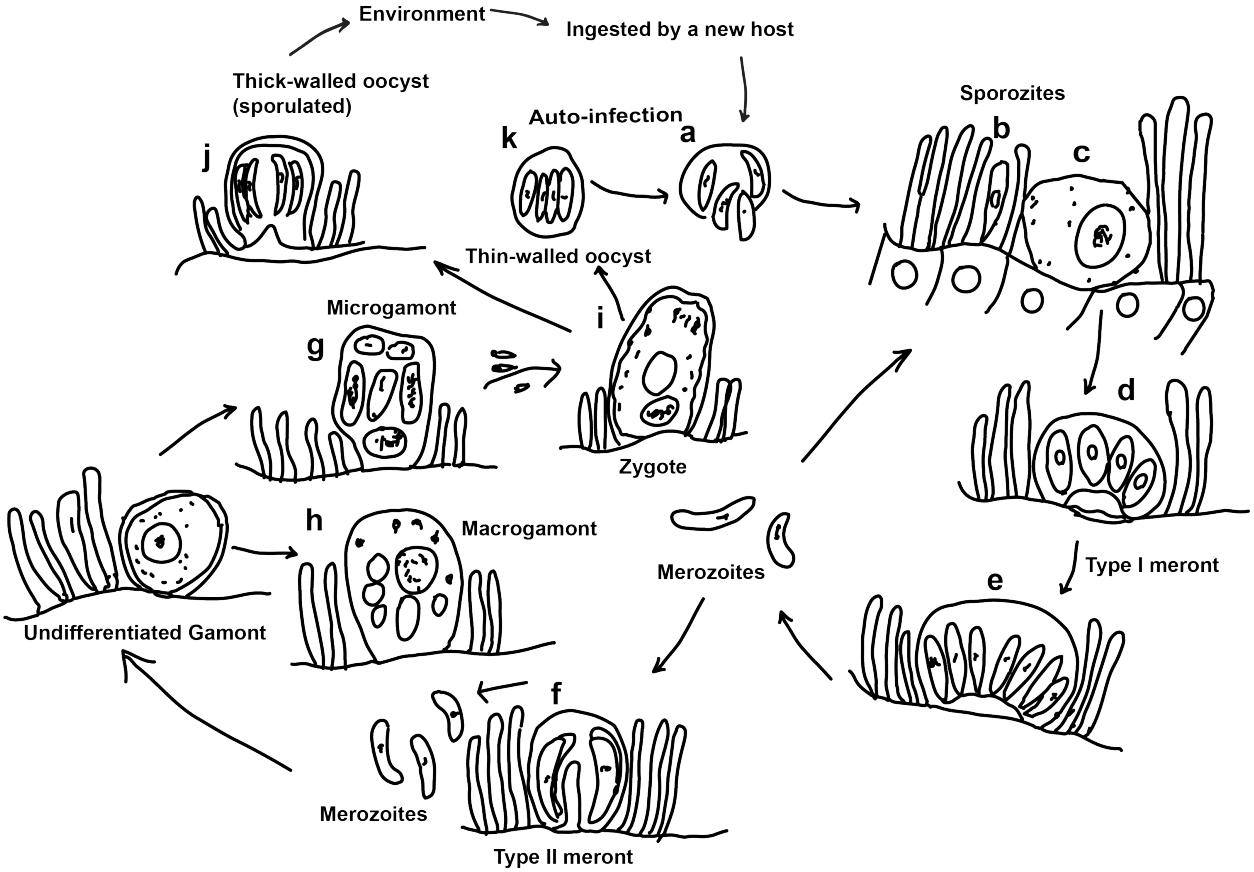

Figure 1.1 Schematic representation of the *C. parvum* life cycle as an example of *Cryptosporidium spp.* life cycle (not to scale, Adapted from (Bouzid et al. 2013)).

1.3 Poorly understood mechanisms of *Cryptosporidium* invasion

1.3.1 Cryptosporidium *oocyst excystation*

Excystation is the essential process for a *Cryptosporidium* oocyst to infect a host cell, but the mechanisms regulating it are not yet fully understood. Although both parasite and host cell factors participate in the excystation process, little is known about the detailed role of each component. It is known that temperature and pH can increase oocyst wall permeability. The passage of oocysts through the stomach and intestines in humans can be mimicked by exposing the oocysts to acid (PH ~2) and then incubating the oocysts with bile salt, proteases, and reducing agent. This process can improve the oocyst excystation in vitro, but the essential factors are unknown since *Cryptosporidium* could also infect other parts of the body in immunocompromised people, for example lungs (Travis et al. 1990, French et al. 1995, Dunand et al. 1997). Incubating the oocysts at 37 °C can achieve maximum (91%) excystation rate, with the excystation rate dropping with a reduction in temperature (Fayer and Leek 1984, Reduker and Speer 1985). Besides pH and temperature, protease, bile salts, reducing agents, and time could influence oocyst excystation, but our knowledge about them is limited. After the activation of sporozoites in oocysts, sporozoite-derived protease is involved in the excystation. Among different proteolytic enzymes, serine and cysteine protease activities peak during the oocyst excystation period. However, only serine protease inhibitors prevent oocyst excystation in a dose dependent manner at the beginning of excystation (Forney et al. 1996). An arginine aminopeptidase (RAP), which cleaves the N-terminal of arginine or alanine, is expressed throughout and after excystation and its activity increases during the excystation process in vitro. Treatment with RAP inhibitor reduces the excystation rate (Okhuysen et al. 1996, Padda et al. 2002). In summary, the oocysts are ingested through contaminated food or water and are

activated upon the rise of the temperature in the stomach, followed by the production of proteases in sporozoites. The out layer of the oocysts, which consist of mainly glycoproteins, is degraded in the corrosive stomach acid, allowing bile salts to pass through, followed by the activation of the sporozoites in the oocysts. The digestive enzymes in the intestine and protease produced by sporozoites weaken the suture area in the oocysts wall, leading to a rupture (Reduker and Speer 1985). The structure of the oocyst wall is not fully understood, but consists of a glycocalyx, a lipid, and a glycoprotein layer, protecting the parasite from chemicals and mechanical stress. The inner layer is mainly composed of eight *Cryptosporidium* oocyst wall proteins (COWPs). Besides COWP1 and COWP8, which haven't been studied much, COWP2-7 are cysteine-rich proteins, forming disulphide bonds to strengthen the inner layer (Bushkin et al. 2013, Spano et al. 1997, Templeton et al. 2004).

1.3.2 Sporozoites attachment and invasion

After the release of sporozoites from oocysts, sporozoites contact with the mucus layer, which has a thickness from 120 μm (small intestine) to 800 μm (colon). How *Cryptosporidium* sporozoites, which only are 3 μm long, go through the barrier is still not fully understood. They may penetrate the mucus layer by mechanical force, use secreted protease, or even some other mechanisms (Moncada et al. 2003, Lidell et al. 2006, Lendner and Daugschies 2014). As a condition to penetrate the mucus layer, it is suggested that sporozoite surface galactose-N-acetylgalactosamine (Gal/GalNAc) lectins bind to galactose-N-acetylgalactosamine of the mucus layer through receptor-ligand interactions. The incubation with Gal/GalNAc or bovine submaxillary mucin before infection inhibits the attachment and/or invasion of cells in vitro (Joe et al. 1998, Hashim et al. 2006).

A 30 kDa Gal/GalNAc lectin (p30) mainly located in the apical region of *C. parvum* sporozoites was discovered, and incubation with p30 in attachment inhibition assays suggest that p30 plays an important role in attachment by forming a protein complex with GP40 and GP900, two heavily O-glycosylated glycoproteins involved in sporozoites attachment that regulate binding (Bhat et al. 2007). GP40 and GP15 are formed by the cleavage of a 60 kDa (GP60) precursor (Strong et al. 2000). GP15 binds to the intestine membrane by a Glycosylphosphatidylinositol (GPI) anchor. The manner in which GP40 binds to cells is dose-dependent and is shed in the moving trails of sporozoites. Antibodies against GP40 inhibit the parasite infection by about 82% in vitro (O'Connor et al. 2007, Cevallos et al. 2000a). GP900 is also a highly glycosylated protein with a putative transmembrane domain and may anchor to the cell membrane after being released from the sporozoites micronemes. Competitive inhibition studies show that GP900 regulates both sporozoite attachment and invasion (Barnes et al. 1998). Another circumsporozoite-like (CSL) glycoprotein binds preferably to epithelial cells, although the gene encoding for CSL remains to be identified (Riggs et al. 1994). Additionally, there are a number of other parasite surface proteins that could inhibit the parasite invasion at certain levels and/or possess immunodominant properties that imply their involvement in parasite-host cell interactions, such as *C. parvum* antigen 2 (CP2), antigen 47 (CP47), CPS-500 and Cpa135 (Riggs et al. 2002, O'Hara et al. 2004, Nesterenko et al. 1999, Riggs et al. 1999, Bonafonte et al. 2000, Perryman et al. 1996). Although more than 20 sporozoite proteins, summarized in Table 1.1, have been identified, the precise roles of these proteins and the mechanisms involved in and regulating the parasite attachment and invasion are poorly understood.

Table 1.1 *Cryptosporidium* receptors and their roles in attachment and invasion adapted from references (Lendner and Daugschies 2014, Borowski et al. 2008, Smith et al. 2005)

Parasite receptors	Location(s)	Characteristic(s)	Putative function(s)	References
CP12	Oocyst surface and apical region of sporozoites	Immunodominant protective effect	Host cell adhere	(Yao et al. 2007, Tosini et al. 2004)
CP21		Immunodominant protective effect		(Yu et al. 2010)
CP2	Sporozoites; host-parasite interface; PVM of intracellular stages and cytoplasm of sexual stages	Up-regulated expression during sexual development	Host cell invasion	(O'Hara et al. 2004)
CP20	Surface of sporozoites and oocysts	DNA vaccine of mice cause immune response	Induced a strong immune response and reduction of oocysts shedding	(Xiao et al. 2011)
CP47	The apical region of sporozoites	Membrane-associated protein; binds to a 57 kDa receptor on host cell surface	Role in attachment in host cells	(Nesterenko et al. 1999)
CPA135	Apical region of sporozoite and maybe a microneme protein	Co-localized with GP900	Secreted by sporozoites during gliding; abundant in excystation; start the parasite invasion	(Tosini et al. 2004)
CPS-500	Sporozoite pellicle	A polar glycolipid	Secreted by sporozoites during gliding	(Riggs et al. 1989, Perryman et al. 1990)
CSL	Apical region of sporozoites and merozoites	Binds an 85kDa protein ligand (CSL-R) on host cells	Blocks parasite invasion in vitro and protects against infection in vivo	(Riggs et al. 1994, Langer and Riggs 1999, Langer et al. 2001)
P30	Apical region of sporozoites	A 30kDa Gal/GalNAc specific lectin; may form a protein complex with GP900 and GP40/15;	Binds host cell surface Gal/GalNAc; Inhibits sporozoites attachment	(Bhat et al. 2007)
Gal/GalNAc lectins (i.e. P30)			Parasite attachment to intestinal mucin; binds host cell Gal/GalNAc	(Joe et al. 1994)
GP40	Apical region of sporozoites	Glycoprotein; O-glycosylated; proteolytic fragments of the same 60kDa precursor protein as GP15; soluble	Shed during sporozoites gliding motility; parasite attachment	(Strong et al. 2000, Cevallos et al. 2000a, Wanyiri et al. 2007b, O'Connor et al. 2007a)

Table 1.1 Continued

Parasite receptors	Location(s)	Characteristic(s)	Putative function(s)	References
GP15	Surface of sporozoites and merozoites; co-localized with GP40	Glycoprotein; O-glycosylated; GPI anchored	Shed during sporozoites gliding motility; sporozoites attachment	(Strong et al. 2000, Cevallos et al. 2000a, Wanyiri et al. 2007a, O'Connor et al. 2007a)
GP900	Apical region of sporozoites; stored in micronemes	Glycoprotein; O-glycosylated; intracellular with small extracellular portion	Binding to intestinal mucin	(Barnes et al. 1998, Petersen et al. 1992)
P23	Sporozoites surface	Reduce infection in mice by its antibody; hyperimmune serum against a part of P23 reduce oocyst shedding	Maybe involved in sporozoites gliding	(Bonafonte et al. 2000, Enriquez and Riggs 1998, Perryman et al. 1999, Wyatt et al. 2000, Wyatt and Perryman 2000, Takashima et al. 2003)
TRAP-C1	Apical complex in sporozoites; probably in micronemes	Contained copies of type I repeat of human platelet thrombospondin (TSP1)	Adhesion protein; secreted by sporozoites during gliding motility;	(Spano et al. 1998, Deng et al. 2002, Okhuysen et al. 2004)
MUC1-7	Apical region of sporozoites	Small mucin sequences identified on chromomosome 2	Infection inhibited by anti-MUC4 antibody	(O'Connor et al. 2009)
CpEF-1α	Apical region of sporozoites	Identified by an antibody that inhibits parasite invasion; Identified EF-1α by MALDI-TOF-MS	Sporozoites invasion	(Matsubayashi et al. 2013, Inomata et al. 2015)
CpClec	Sporozoites apical surface	Mucin like glycoprotein with C-type lectin domain (CTLD)		(Bhalchandra et al. 2013)
Cryptopain-1	Within oocysts and meronts	Papain family enzyme	Possibly involved in parasite invasion	(Na et al. 2009, Ndao et al. 2013)
Cryptostatin	Diffuse with oocysts and meronts	Inhibitor of cysteine proteases		(Kang et al. 2012)
Heparin		Binds with *C. parvum* Elongation factor 1α (CpEF-1α)	Parasite invasion	(Inomata et al. 2015)
MEDLE-2	Belongs to *Cryptosporidium*-specific MEDLE family of secreted protein	Distribute on the sporozoites and development stages	Potentially involved in the *C. parvum* invasion	(Li et al. 2017)

1.3.3 Host cell response to Cryptosporidium *infection*

The morphological changes of the parasites at the infection sites have been extensively studied (Amadi et al. 2002, Vetterling et al. 1971, Marcial and Madara 1986, Lumb et al. 1988, Umemiya et al. 2005). The apical region of the parasite attaches onto the luminal surface of the host intestine among the microvilli, which elongate along the surface of the parasite, followed by the parasite attachment. A dense band is formed within the host cell cytoplasm and then both the parasite and host cell membrane undergo morphological changes, including the transformation of a banana-shaped sporozoite to a nearly round-shaped trophozoite and the formation of host cell derived PVM at the infection site. The PVM contains an intracellular parasite and is attached to the host cell plasma membrane by a unique electron-dense (ED) structure padded with a layer of filamentous network (**Figure 1.2**). As seen in Figure 1.2, the developing intracellular parasite is covered by the host cell and directly connected via an electron dense (ED) structure. The ED structure is typically associated with a feeder organelle (FO) in the parasite and with an F-actin rich filamentous network in the host cell. The host cell origin actin filamentous network was validated by enhanced expression of the β-actin green fluorescent protein (GFP) of a host cell line, which were present at the infection sites and visualized using fluorescence microscopy. The same result was observed by employing phalloidin staining of *Cryptosporidium*-infected cells: a circular, plaque-like collection of actin filaments at every infection site and a parasite PVM composed of host cells derived actin filaments (Elliott and Clark 2000).

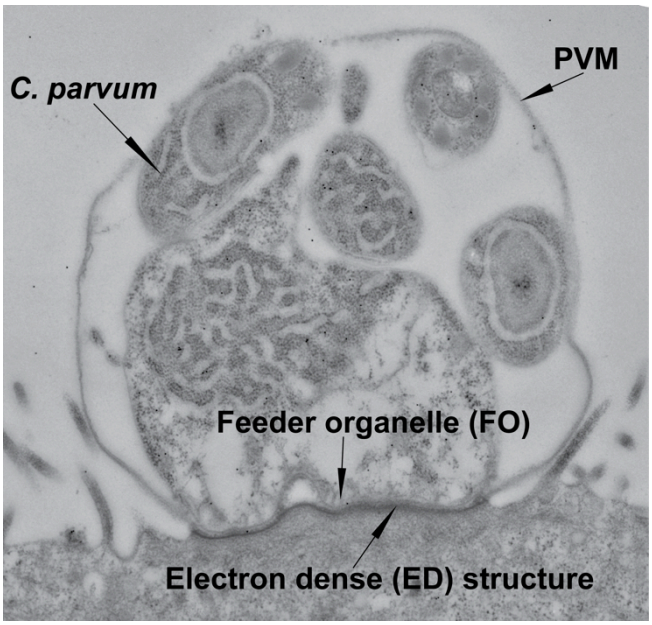

Figure 1.2 Diagram of the interactions between *Cryptosporidium* and host intestine epithelial cell.

Actin is known to interact with cell plasma membranes and plays a critical role in remodeling membranes and in maintaining cell shape and polarity (Nelson 2009). Several researchers have suggested the active role of host cell actin in parasite invasion, and early infection studies using host cells pretreated with pharmacological inhibitors showed that phosphatidylinositol-3-kinase (PI3K) was involved in *Cryptosporidium* early invasion (Elliott and Clark 2000, Forney et al. 1999). *C. parvum* employs actin branching and Arp2/3 complex nucleation machinery to induce actin polymerization (Mullins et al. 1998, Elliott et al. 2001). Further studies show that several host cell factors and signaling pathways are involved in modeling actin reorganization during *Cryptosporidium* infection including c-Src-dependent tyrosine phosphorylation for the accumulation of cortactin and phosphatidylinositol-3-kinase (PI3K), as well as frabin-mediated activation of CDC42 for the recruitment of Neural Wiskott-Alrich syndrome protein (N-WASP) (Chen et al. 2003, Chen et al. 2004b, Chen et al. 2004a). For CDC42 activation, it was reported that N-WASP was activated by a phosphorylation cascade,

followed by recruitment/activation of Arp2/3 (Chen et al. 2004a). Another study showed that host cell integrin α2 (ITGA2) was upregulated during the parasite infection and a reduction of infection was observed in HCT-8 cell lines with stable knockdown of ITGA2 gene, indicating its involvement in interacting with *Cryptosporidium* during infection (Zhang et al. 2012a). The host factors and pathways discussed above may be directly or indirectly associated with the regulation and/or remodeling of F-actin, but the information is highly fragmented. The exact molecular pathways regulating the actin remodeling in host cells remain largely unresolved.

1.4 The many roles of eukaryotic elongation factor 1α

The canonical role of eukaryotic elongation factor 1α (eEF1α) is the elongation of polypeptide chains. eEF1α is also a central regulator for many other cellular activities, including heat shock regulation, actin bundling, nuclear export, protein degradation, and apoptosis.

1.4.1 The classic role of eEF1α

Eukaryotic elongation factor 1α (eEF1α) is an isoform of the α-subunit of the EF1 complex and is a GTP binding protein. After it binds GTP, the complex delivers the aminoacyl-tRNAs to A site in the ribosome for codon-anticodon recognition, followed by GTP hydrolyzed to GDP and the release of eEF1α from the ribosome. Free eEF1α then binds with nuclear exchange factor to exchange GDP for GTP causing protein reaction and the start of the next cycle (Li et al. 2013).

1.4.2 eEF1α is involved in heat shock response

Several studies show that eEF1α plays a role in heat shock response to deal with environmental stresses including starvation and elevated high temperature (Shamovsky et al. 2006, Kugel and Goodrich 2006, Vera et al. 2014). In mammalian cells, eEF1α interacts with

heat shock factor 1 (HSF1), which regulates the heat shock response by binding the promoter region of unregulated genes related heat shock elements (Kugel and Goodrich 2006). The interaction between eEF1α and HSF1 is enhanced upon stress (Vera et al. 2014). However, without stress, eEF1α binds the promoter region of heat shock proteins repressing gene translation (Vera et al. 2014).

1.4.3 eEF1α and actin bundling

Evidence has been produced from several laboratories that protein translation function is linked with the cell cytoskeleton (Kim and Coulombe 2010, Gross and Kinzy 2007, Stapulionis et al. 1997). Several translational proteins are associated with the cell cytoskeleton and efficient translation in mammalian cells depends on intact actin filaments (Kim and Coulombe 2010, Gross and Kinzy 2007). The cytoskeleton also ensures the efficiency of translational machines by spatially separating them in a reasonable concentration (Martin and Ephrussi 2009).

The first report that eEF1α was an actin-binding protein was from slime mold (Yang et al. 1990). eEF1α exists in two forms: monomeric and dimeric. Researchers discovered through electron microscopy and cosedimentation assays that only dimeric eEF1α could bundle actin filaments, dimeric eEF1α is regulated by Ca^{2+} /Calmodulin, and low concentrations of Ca^{2+} /Calmodulin promoted the formation of eEF1α dimers and actin filament bundling (Liu et al. 1996, Bunai et al. 2006).

1.4.4 eEF1α and the nuclear export process

Research demonstrated that the reduced expression of eEF1α or mutations in eEF1α domain II in mutant yeast displayed defects in nuclear export of aa-tRNA (Grosshans et al. 2000). Further study showed that eEF1α participated in nucleus export depending on the transcription of proteins from the nucleus, which is distinct from protein synthesis (Khacho et al.

2008). Researchers also found that eEF1α could be detected in the nucleus of budding yeast with mutations in the nucleus transporter, indicating that eEF1α could access the nucleus (Murthi et al. 2010).

1.4.5 eEF1α and apoptosis

Apoptosis is programmed cell death and is a highly regulated set of events to eliminate damaged, unhealthy, or unnecessary cells. Experiments have shown that the expression level of eEF1α in mouse fibroblasts is associated with the rate of apoptosis: the higher the concentration of eEF1α, the higher the cell death rate (Duttaroy et al. 1998). In another experiment, eEF1α was isolated as a factor, which promotes cell survival after the withdrawal of the growth factor in a pro-B cell line (Talapatra et al. 2002). Further research showed that the contradictory observations may be due to the two differentially expressed isoforms of eEF1 in vertebrates: eEF1α1 expression was involved in differentiation and prevented cells from apoptosis in cultured myoblasts, while eEF1α2 expression promoted apoptosis (Khalyfa et al. 2001, Lee et al. 1992, Ruest et al. 2002).

1.4.6 eEF1α and viral propagation

Viruses rely on host cells to replicate and propagate. Many viruses have evolved to use eEF1α in different ways. In the yellow mosaic virus, eEF1α binds an aa-tRNA-like element in the virus genome (Matsuda et al. 2004). In the West Nile and tobacco mosaic viruses, eEF1α interacts with the virus RNA and RdRP protein (Blackwell and Brinton 1997, Davis et al. 2007). By mutating the eEF1α-binding site in the West Nile virus genome, researchers found a decrease in virus minus strand synthesis, causing a reduction in viral propagation (Davis et al. 2007). Defective viral replication was found in brew yeast *Saccharomyces cerevisiae* expressing a mutated eEF1α (Yamaji et al. 2010).

1.4.7 eEF1α and protein degradation

It seems counterintuitive that eEF1α plays a role in protein degradation. However, the high concentration of eEF1α in cells may indicate a potential role for protein quality control and co-translational degradation. Researchers found that eEF1α was a required factor for the degradation of specific protein families (Gonen et al. 1994). eEF1α was also found to suppress growth defects caused by gene deletion in proteolytic pathways, and regulate protein degradation by connecting unfolded proteins with proteasome (Chuang et al. 2005).

1.5 Potential role of *C. parvum* elongation factor 1α (CpEF1α) in regulating the F-actin remodeling in host cells

Currently, for *C. parv*um infection, only a few host cell factors are thought to possibly regulate and/or participate in the remodeling of F-actin at the infection site, such as the Arp2/3 complex actin nucleator, N-WASP, and the vasodilator-stimulated phosphoprotein (VASP) (Forney et al. 1999, Mullins et al. 1998, Elliott et al. 2001, Chen et al. 2003, Chen et al. 2004b, Chen et al. 2004a). eEF1α can both bind and bundle actin filaments in vitro, and this activity has been evolutionarily conserved (Yang et al. 1990, Liu et al. 1996, Bunai et al. 2006, Demma et al. 1990). For example, *C. parvum* EF1α (CpEF1α) (GenBank accession number: XP_001388344; GeneID: cgd6_3990) shares 72% amino acid identity with human EF1α (HsEF1α), implying that CpEF1α may be able to interact with human actin (**Figure 1.3**). As shown in Figure 1.3, positions containing identical amino acids in all species are shaded and marked by asterisks (*), and positions containing high similarities are indicated by carets (^). The GenBank accession number for each species tested are as follows: *Cryptosporidium parvum,* XP_001388344; *Toxoplasma gondii,* XP_002369268; *Plasmodium falciparum,* XP_001350281; *Candida albicans,* XP_711899; *Saccharomyces cerevisiae,* NP_009676; *Zea mays,* NP_001288465;

Homo sapien, NP_001949; *Drosophila melanogaster,* NP_477375; *Giardia lamblia,* XP_001704529; and *Leishmania major,* XP_001682258. As mentioned early, host cell actin reorganization plays an active role in the parasite invasion process (Elliott and Clark 2000). Thus it is possible that CpEF1α is involved in the *C. parvum* invasion process by interacting with human actin filaments.

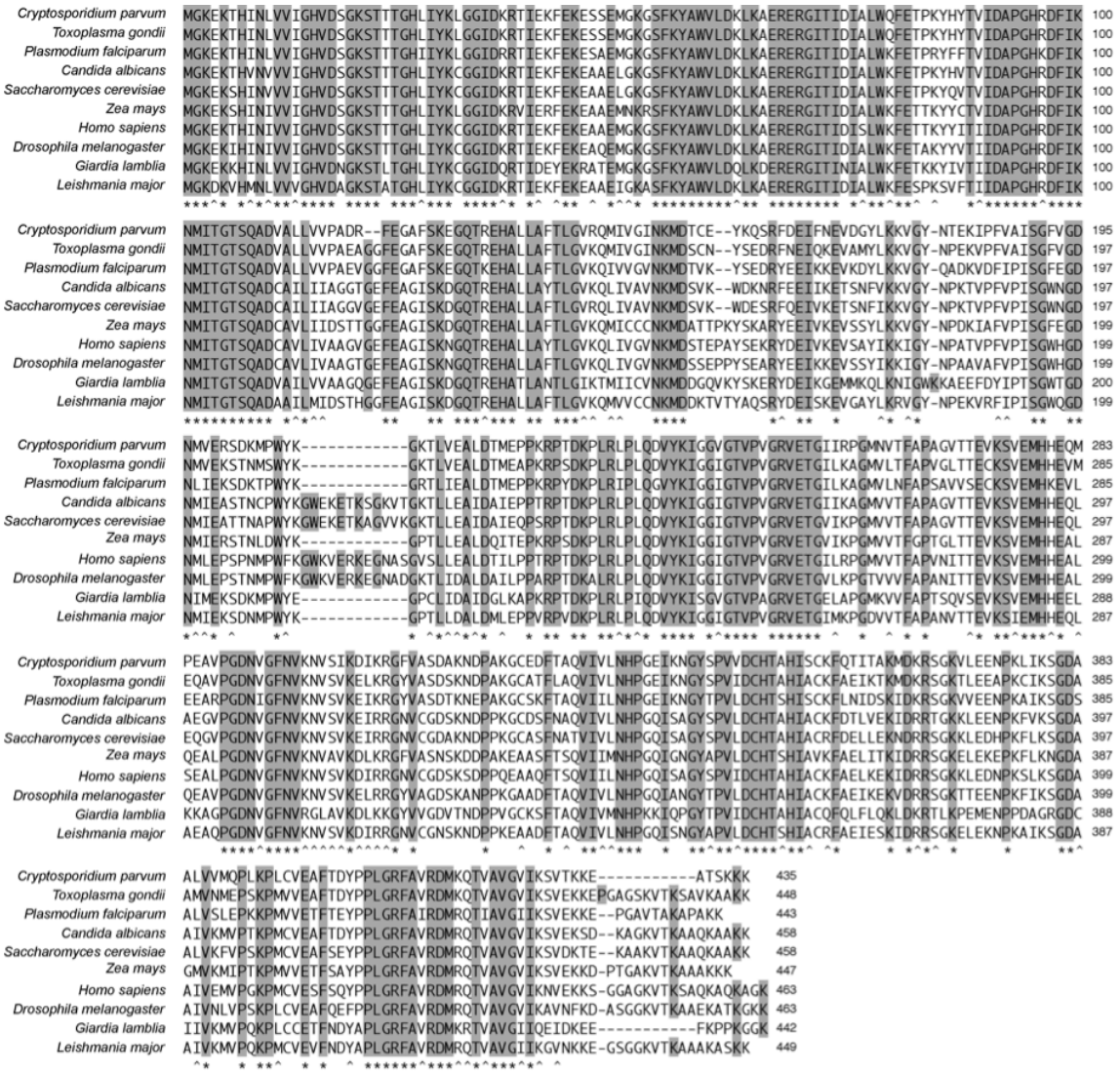

Figure 1.3 Multiple amino acid sequence alignment of eEF1α from selected eukaryotic species including apicomplexans, other protozoa, fungi, plants, and animals.

1.6 Summary

Cryptosporidium infects both humans and animals to cause cryptosporidiosis. The pathogenesis and the molecular interactions between the parasite and host cells remain poorly understood; how the parasites invade host epithelial cells and establish infection, and the proteins and pathways involved in the invasion remain to be explored. In this study, we obtained and characterized the host cell mutants that are partially resistant to the parasite infection. These host cell mutants will allow us to use transcriptomics and proteomics approaches to identify host cell candidate genes critical to the establishment of the *Cryptosporidium* infection. The role of CpEF1α in regulating the reorganization of F-actin proteins in humans during the invasion process was also characterized. The data generated in this study will have great potential to expand our understanding on the molecular mechanisms underlying the parasite infection.

CHAPTER II

CHARACTERIZATION OF HOST CELL MUTANTS SIGNIFICANTLY RESISTANT TO *Cryptosporidium parvum* INFECTION*

2.1 Introduction

Cryptosporidium is a genus of enteric protozoan parasites that infect both humans and animals (Bonafonte et al. 1997, Ajjampur et al. 2010, Fletcher et al. 2012). Humans are mainly infected by *Cryptosporidium parvum* (zoonotic) and *C. hominis* (human-specific), in which children, elderly, and individuals with weakened immune systems are at a higher risk of severe to deadly infections (Checkley et al. 2015, Leitch and He 2012, Ajjampur et al. 2010). Currently, only nitazoxanide (NTZ) has been approved by the Food and Drug Administration (FDA) in the United States to treat cryptosporidiosis in immunocompetent people, whereas no drugs are approved for use on immunocompromised patients or on animals (Ollivett et al. 2009, Checkley et al. 2015, Lal et al. 2015).

Cryptosporidium parasites have a direct life cycle and are transmitted by oocysts from the environment via the fecal-oral route. When oocysts are ingested by humans or animals, the four sporozoites contained in each oocyst will be released in the gastrointestinal track to invade gastric (e.g., *C. muris*) or intestinal (e.g., *C. parvum* and *C. hominis*) epithelial cells (Prystajecky et al. 2014). The morphological changes of the parasites at the infection sites have been extensively studied, but the mechanisms involved in regulating the parasite attachment and invasion are poorly understood. In the host cells, it is known that parasite protein CSL binds to

---

· This research was reprinted from Yu, X., Zhang, H. & Zhu, G. 2017, Characterization of Host Cell Mutants Significantly Resistant to *Cryptosporidium parvum* Infection. *J Eukaryot Microbiol,* **64:**843-849, with premission from John Wiley and Sons.

an 85-kDa host cell membrane protein (designated as CSL-R), but the identity of CSL-R is unclear. Several other host cell factors and pathways have been shown to possibly be involved in the parasite invasion, including c-Src-dependent tyrosine phosphorylation for the accumulation of cortactin and phosphatidylinositol-3-kinase (PI3K) and frabin-mediated activation of CDC42 for the recruitment of Neural Wiskott-Alrich syndrome protein (N-WASP) (Chen et al. 2003, Chen et al. 2004b, Chen et al. 2004a). A fairly recent study also showed that host cell integrin α2 (ITGA2) might be involved in interacting with *Cryptosporidium* during infection (Zhang et al. 2012a). These studies provide important clues on the host cell pathways involved in the parasite infection, but the "key" host cell proteins that directly interact with the parasite during the invasion and development still remain undefined.

In the present study, we have produced 43 mutated host cell lines derived from parent HCT-8 cells by UV irradiation and identified three cell mutants showing significant resistance to the infection by *C. parvum* (i.e. A05, B08 and B12 cell lines with up to ~50% reduction of parasite infection). The three cell mutants exhibit different mechanisms of resistance to the parasite infection, mainly impairing the parasite attachment and invasion (A05), or mainly affecting the parasite intracellular development (B08 and B12). These host cell mutants may serve as important reagents for discovering genes and proteins critical to the cryptosporidial infection by forward genetic approaches such as transcriptomic and proteomic analyses.

2.2 Materials and Methods

2.2.1 Parasite, host cells, and general in vitro culture method

The IOWA-1 strain of *C. parvum* was used in all experiments. Fresh parasite oocysts were purchased from Bunch Grass Farm (Deary, Idaho, USA) and stored in phosphate-buffered saline (PBS, pH = 7.4) at 4 °C. Before use, oocysts were suspended in water and treated with

10% Clorox (~0.5% sodium hypochlorite) for 5 min on ice, followed by ≥5 washes with water by centrifugation (2,000 x g, 10 min each). After the final wash, oocysts were suspended in PBS, counted using a hemocytometer, and stored at 4 °C until use. All experiments used oocysts that were ≤3-month old. Oocysts were used directly to infect host cells cultured in vitro as described below, or induced to release free sporozoites by an in vitro excystation procedure. Excystation was prepared by incubating oocysts in PBS containing 0.25% trypsin and 0.5% taurodeoxycholic acid at 37°C for 1 h, quenched by an equal volume of 10% bovine serum albumin (BSA) in PBS, followed by ≥3 washes with PBS.

HCT-8 cells derived from ileocecal colorectal adenocarcinoma (ATCC # CCL-224) were used to host the cultivation of *C. parvum* in vitro in RPMI-1640 medium supplied with penicillin and streptomycin (100 U/mL each), 3 g/L sodium bicarbonate, 1 g/L glucose, and 10% fetal bovine serum. In a typical in vitro assay, HCT-8 cells were seeded in 24- or 96-well plates with culture medium, and incubated at 37°C under 5% CO_2 atmosphere. After cultivation overnight and when cells reached to ~90% confluence, *C. parvum* oocysts, or free sporozoites at a specified parasite to host cell ratio, were added into plates to infect cells for 3 h (oocysts) or 2 h (sporozoites), followed by a medium exchange to remove parasites which failed to invade host cells. Invaded parasites were allowed to grow for various times before proceeding to subsequent experiments as specified.

2.2.2 UV irradiation of HCT-8 cells and cell cloning

HCT-8 cells were seeded into a 24-well plate (5×10^4 cells/well) and allowed to grow overnight and reach ~80% confluence. On the following day, cells were detached and subjected to UV-B irradiation at an ID_{20} dose, i.e., 8 J/m^2 based on Busch et al (Busch et al. 1980). After UV irradiation, cells were diluted with culture medium (200 μL per cell) for cultivation in 96-

well plates (200 µL/well). Cultured cells were observed daily to identify wells that contained single cell colonies, and allowed to grow for two weeks until they reached full confluence. Culture medium was changed every three days. Cloned cell mutants were propagated in 24-well plates or 25 cm^2 cell culture flasks, cryopreserved, and/or used as host cells to grow *C. parvum* in vitro.

2.2.3 Phenotypic screening of cell lines by 18 h in vitro infection assay

Individual mutant cell lines derived from parent HCT-8 cells (wild-type, WT) were screened for their susceptibility to the *C. parvum* infection by an 18 h in vitro infection assay in comparison with that of the wild-type (WT) parent HCT-8 cells. Cells were detached from flasks, seeded into 48-well plates (7×10^4 cells/well), and incubated overnight at 37°C until ~90% confluence. Host cells were then inoculated with 1×10^4 oocysts per well (oocysts to host cell ratio = ~1:10). Parasites were allowed to undergo excystation and invasion into host cells for 3 h at 37°C, followed by a medium exchange to remove free parasites and oocysts walls. Parasite-infected cells were then incubated at 37°C for additional 15 h (total 18 h infection time). The number of seeded cells per well was determined based on their growth rates to ensure that all cell lines reached a similar confluence by the time of inoculation with *C. parvum* oocysts. The oocyst to host cell ratio (i.e., 1:10) was also much lower than that used in a typical drug efficacy assay (i.e., 1:2; e.g., see (Fritzler and Zhu 2012, Zhang et al. 2015) to further minimize the host cell density effects on the parasite infection as described in more details later.

At 18 h post-infection time, cell lysates were prepared as described (Zhang and Zhu 2015). Culture plates were centrifuged for 5 min at 1,000 RPM in a plate centrifuge to ensure that all cells and potential free merozoites in the medium were firmly settled down on the bottom of the plates. Medium was removed and washed with PBS twice, with plates being centrifuged

after each wash. Cells were then lysed by adding 200 µL of ice-cold Bio-Rad iScript qRT-PCR sample preparation reagent (iScript lysis buffer) (Bio-Rad laboratories, Hercules, CA). Plates were sealed with plastic films and vortexed for 20 min using multi-tube Vortexer at speed 7 (VX-2500, VWR International, Radnor, PA), followed by incubation at 80°C for 15 min. After incubation, plates were centrifuged for 5 min at 1,000 RPM to settle down cell debris. Supernatants were subjected to 1:10 dilution with RNase/DNase-free water for use as templates in qRT-PCR or stored at -80°C until use.

The parasite loads were evaluated by detecting the levels of 18S rRNA transcripts from *C. parvum* (Cp18S) by real-time quantitative RT-PCR (qRT-PCR) using a Bio-Rad CFX96 Touch Real-Time PCR Detection System using a protocol similar to the one described earlier (Zhang and Zhu 2015). Each reaction (15 µL final volume) contained 4.5 µL diluted cell lysate, 7.5 µL One Step SYBR Green master mix (Quanta Biosciences, Gaithersburg, MD), 0.15 µL of RT-master mix, 2.35 µL water, and 0.5 µL of primer containing a mixture of Cp18S-1011F (5'-TTGTTC CTT ACT CCT TCA GCA C-3') and Cp18S-1185R (5'-TCC TTC CTA TGT CTG GAC CTG-3') (each at 100 µM). The thermal cycles started with the synthesis of cDNA at 50°C for 20 min, followed by the inactivation of reverse transcriptase at 95°C for 5 min, and 40 cycles of PCR amplification at 95°C for 10 s and 58°C for 30 s. At least two technical replicates were included for each sample. Melting curves were analyzed at the end of PCR amplification to assess the quality and specificity of the reactions.

The relative parasite loads based on the cycle threshold (C_T) values of Cp18S were computed similarly as previously described (Zhang and Zhu 2015), but the levels of human 18S rRNA transcripts were not included in the analysis to avoid errors caused by variations of growth rates of individual cell lines. Briefly, ΔC_T values between individual samples (mean of C_T values

from technical replicates) and WT cells (mean of C_T values from technical and biological replicates) were first determined (i.e., $\Delta C_T = C_{T[mutant]} - C_{T[WT]}$). Standard curves were generated by plotting ΔC_T values against the common logarithm of the oocyst numbers used to infect cells for 18 h (i.e., 2,500, 5,000, 10,000 and 20,000 oocysts/well), and linear regression was performed to obtain the slope value for computing PCR efficiency. The relative parasite loads were calculated using the following equation (Zhang and Zhu 2015, Cai et al. 2005):

$$\text{Relative Growth (\%)} = (10^{(1/\text{slope})*\Delta C_T)})*100 \quad (1)$$

$$\text{Growth Reduction (\%)} = (1 - 10^{(1/\text{slope})*\Delta C_T)})*100 \quad (2)$$

2.2.4 Detailed phenotypic analysis of selected cell mutants

After several mutant cell lines with significantly decreased or increased infection rates were identified by screening, we further evaluated their susceptibility to the *C. parvum* infection by the qRT-PCR as described above. Cell lysates were prepared after 3 h inoculation of *C. parvum* oocysts for assessing parasite invasion or after a total of 18 h infection (3 h invasion, followed by removal of free parasites and incubation for additional 15 h) for assessing early stage of intracellular development.

The parasite invasion is a two-step process, including the attachment of sporozoites onto the host cell surface and the entry of attached sporozoites into host cells. The effects of cell mutations on these two steps were investigated through immunofluorescence microscopy using a previously described but slightly modified protocol (Chen and LaRusso 2000). Briefly, WT and selected mutants were seeded into a 24-well plate containing poly-L-lysine-coated glass coverslips and grown to ~90% confluence. At this point, cell monolayers were fixed with 4% paraformaldehyde in PBS for 20 min at 4°C for the attachment assays or kept live (unfixed) for the invasion assay. After three washes with PBS, host cells were incubated with excystated

sporozoites (2×10^5/well) for 2 h, followed by fixation with 4% paraformaldehyde for 20 min at 4°C. Fixed cells were washed three times with PBS, followed by 5 min treatment of 1.0% Triton-X100 and a final wash by PBS. The monolayers were mounted with Fluoroshield with 4',6-diamidino-2-phenylindole (DAPI) histology mounting medium (F6057 Sigma). The sporozoites that attached onto or invaded into host cells were counted under an Olympus BX51 research microscope with appropriate filter sets and expressed as the number of sporozoites per field under a 40× objective lens. The experiments were repeated at least three times, each containing at least three biological replicates. For each biological replicate, 15 randomly selected microscopic fields were counted and averaged for subsequent statistical analysis by Student's *t*-test for significance between individual mutants and WT cell lines.

We also examined the general morphological features of selected cell lines. Cells were grown on coverslips in 24-well plates for various times and fixed with 4% paraformaldehyde. After three washes with PBS, cells were washed and permeabilized with 0.1% Triton X-100 in PBS for 5 min, followed by three washes with PBS. Samples were then incubated with rhodamine phalloidin (1:300 dilution; Cytoskeleton Inc.) for 1 h. After three more washes with PBS, samples were mounted onto glass slides with SlowFade mounting medium containing DAPI (Molecular probe, Invitrogen). All incubation and wash steps were performed at room temperature. Samples were then examined using a Zeiss Axioplan 2 microscope with appropriate filter sets (i.e., $\lambda_{ex}/\lambda_{em}$ = 535 ± 20 nm/585 ± 20 nm for rhodamine, and $\lambda_{ex}/\lambda_{em}$ = 355 ± 20 nm/460 ± 20 nm for DAPI). Images were captured with an Axiocam HR CCD Digital Camera.

Size measurements were conducted using ImageJ program (v1.51k with JAVA 1.6.0_65) (https://imagej.nih.gov/ij/index.html) on adherent cells grown on coverslips (~30% confluence) and stained with rhodamine and DAPI. The image contrast was adjusted to allow edge selection

on individual cells and nuclei. The area of cell plasma was calculated as the difference between the measured areas of the entire cell minus the measured area of the cell nucleus. Minimums of 85 cells were measured for each cell line. Statistical significance between individual mutants and WT cells was determined by two-tailed Student's *t*-test.

2.3 Results and Discussion

After UV irradiation of HCT-8 cells, we obtained 43 cloned cell lines (mutants) that were propagated in vitro and cryopreserved at various passages. These cell mutants were evaluated using a qRT-PCR assay for their susceptibilities to the infection by *C. parvum* in vitro. In this assay, individual cell mutants and parent HCT-8 cells were allowed to grow in 48-well plates to ~90% confluence and inoculated with *C. parvum* oocysts at a parasite to host cell ratio at 1:10. The purpose of starting with more host cells than a typical drug assay (i.e., ~90% vs. ~80% in confluence of cells) and a smaller number of parasites (i.e., 1:10 vs. 1:2 oocysts to host cell ratio) was to minimize the potential effect of host cell density variations on the parasite infection as individual mutants might grow at slightly different rates. The number of seeded host cells were also adjusted based on their growth rates to ensure they reached to nearly full confluence at the time of inoculation of *C. parvum* oocysts. For the same reason, parasites were allowed to grow for a total of 18 h, rather than 44 h (i.e., from inoculation to the preparation of cell lysates for qRT-PCR assay) to prevent host cells from growing overly disproportional between individual cell lines. After 18 h of infection in vitro, *C. parvum* would typically grow into the late stage of first generation of merogony or early stage of second generation of merogony (i.e., first or second parasite cell cycle), which was sufficient for phenotypic screening of host cells on their susceptibilities to the parasite invasion and early stage of intracellular growth.

Primary screening revealed that most of the 43 mutant cell lines retained similar levels of

susceptibility to the parasite infection in comparison to the WT HCT-8 cells (**Figure 2.1**). However, three cell lines displayed significantly reduced susceptibility (i.e., A05, B08 and B12 with relative growth rates at 58.3%, 54.5% and 71.2%, respectively; *p*-values <0.001 by two-tailed Student's *t*-test), while one cell mutant displayed an increased susceptibility (i.e., D10 at 155.1%; *p*-values <0.001) (**Figure 2.1**). A secondary screening was performed on these four mutants, together with the WT cells and one mutant showing no significant change in susceptibility (i.e., A19 at 96.1%) as controls. In the secondary screening, the mutants A05, B08 and B12 showed similar levels of resistance to infection as observed in the primary screening (**Figure 2.1**, open circles). However, although mutant D10 retained a higher level of susceptibility, it was not at the same level as shown in the primary screening (**Figure 2.1**). Subsequent analysis indicated that the phenotypic features of the five mutants were stable and capable of maintaining similar levels of susceptibilities to the *C. parvum* infection after more than 6 months of propagations in vitro (i.e., the relative parasite growth rates in A05, B08, B12, D10, and A19 cells were mostly at ~50-60%, ~60-70%, ~75-80%, ~110-125%, and 95-105%, respectively).

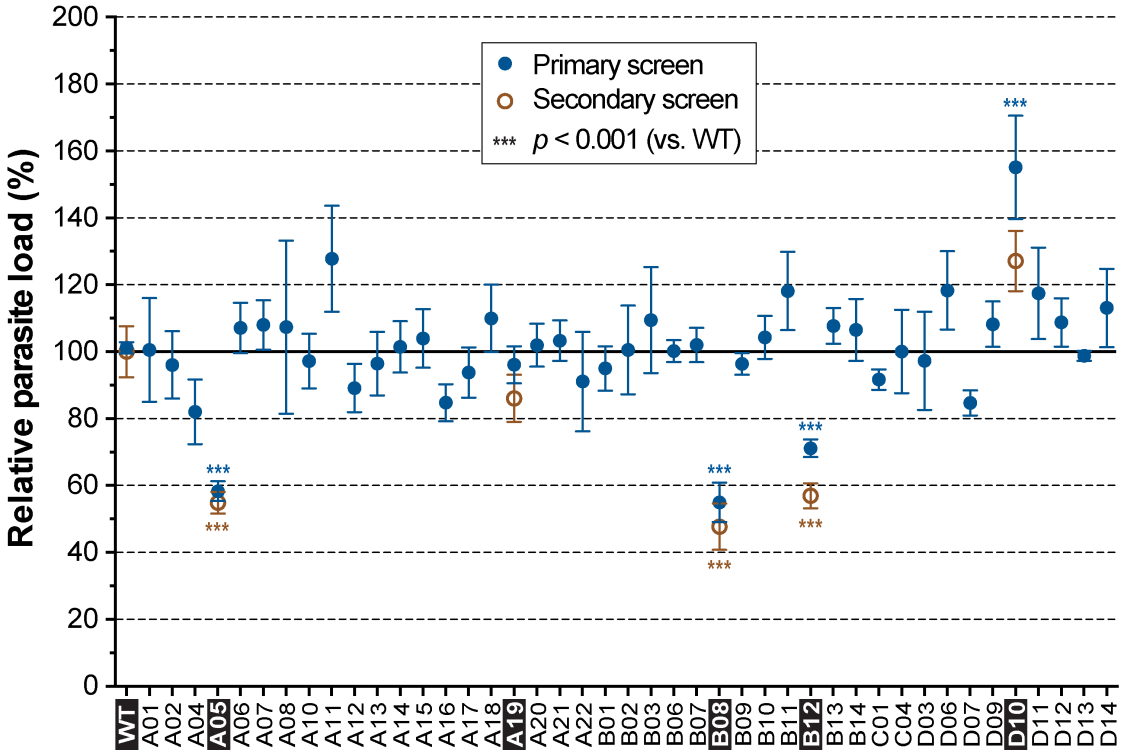

Figure 2.1 Screening of the 43 cell lines (mutants) derived from the wild-type (WT) HCT-8 cells by UV-irradiation for their susceptibility to the infection *by Cryptosporidium parvum* in vitro using an 18-h infection assay.

After determining that A05, B08 and B12 cell lines were significantly resistant to the *C. parvum* infection by the 18-h infection assay, we investigated whether the *C. parvum*-resistant phenotype in the three cell lines was attributed to the resistance of cells to the parasite invasion using a 3 h invasion assay by qRT-PCR, together with the 18 h infection assay for comparison. The 3 h invasion assay revealed that A05 cells were highly resistant to the parasite invasion (i.e., the relative parasite invasion rate = 68.2%, p <0.001 vs. WT cells), whereas B08 and B12 cells displayed no statistically significant differences in the invasion rates (i.e., B08: 91.2%, p = 0.21; and B12: 110.5%, p = 0.16) (**Figure 2.2A**). In the meantime, the 18 h infection assay reconfirmed the statistically significant resistance to the parasite infection in cell lines A05 (57.2%; p <0.001), B08 (66.8%; p <0.001) and B12 (80.6%; p <0.05). Additionally, the

reference cell lines A19 and D10 displayed no significant differences in both 3 h invasion and 18 h infection assays although slight increases in invasion and growth were observed in cell line D10 (**Figure 2.2A**).

Assays were also performed to determine whether the invasion-resistance in A05 cells was a result of the blockage of parasite attachment onto or the entry into the host cells. A05 cells and other cell monolayers were either fixed with paraformaldehyde prior to the inoculation of free sporozoites to allow the attachment, but not the entry of the parasites into host cells (attachment assay), or kept live (unfixed) to allow both attachment and entry (invasion assay). The relative rates of invasion of *C. parvum* sporozoites into live host cells or their relative rates of attachment onto fixed host cells were measured at 2 h post-inoculation time. In these assays, A05 cells displayed significant reductions in both the attachment and the invasion by *C. parvum* sporozoites (i.e., relative levels at 71.6% and 73.4%, respectively; $p < 0.001$ in both assays), while all other mutant cell lines showed no significant changes in both attachment and invasion rates (**Figure 2.2B**). Overall, the parasite invasion rates determined by microscopy (**Figure 2.2B**) and by qRT-PCR (**Figure 2.2A**) were comparable, although there were statistically insignificant variations on the invasion rates for A05, B08 and B12 cell lines between the microscopically counting and qRT-PCR assays.

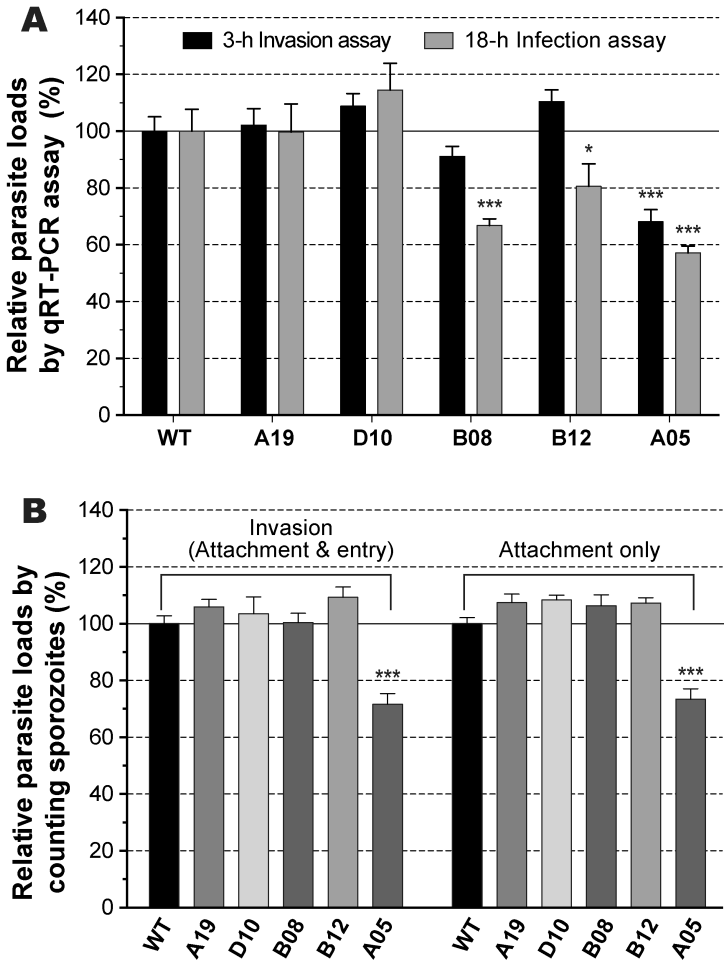

Figure 2.2 Relative rates of invasion or attachment of the *Cryptosporidium parvum* on the wild-type (WT) HCT-8 cells and five mutant cell lines.

Immunofluorescence microscopic analysis revealed that the two cell lines with "normal" unaltered susceptibility to *C. parvum* (i.e., D10 and A19) shared similar morphology with the parent HCT-8 cells (**Figure 2.3**; left panel), although D10 cells were significantly stretched out than other cell lines as indicated by the cell sizes (**Figure 2.4A**). The morphology of the three *C. parvum*-resistant cell lines (i.e., A05, B08 and B12) altered significantly from the parent HCT-8, D10, and A19 cells, as the cell clusters were generally less stretched out on the surface of the plates and had smaller cytoplasmic areas than the other three cell lines (i.e., smaller cytoplasm to cell ratio) (**Figure 2.4B)**. More significantly, the cell-to-cell connections were generally loose,

leaving apparent gaps between neighboring cells (**Figure 2.3**). It is also noticeable that B08 and B12 cells were moderately to highly defective in cell edge extension, leading to the formation of numerous small curled actin-rich membrane nodes in B08 and relatively large membrane folds in B12 cells (**Figure 2.3**). These observations imply that the three parasite-resistant cell lines have certain levels of membrane proteins deficiency that affect the cell connection, edge growth, and/or adhesion. Identification of mutated gene encoding of membrane proteins in these cell mutants, particularly in the A05 mutant, will provide us a set of candidate genes for individual testing of their direct roles in the attachment/invasion of *Cryptosporidium* parasites.

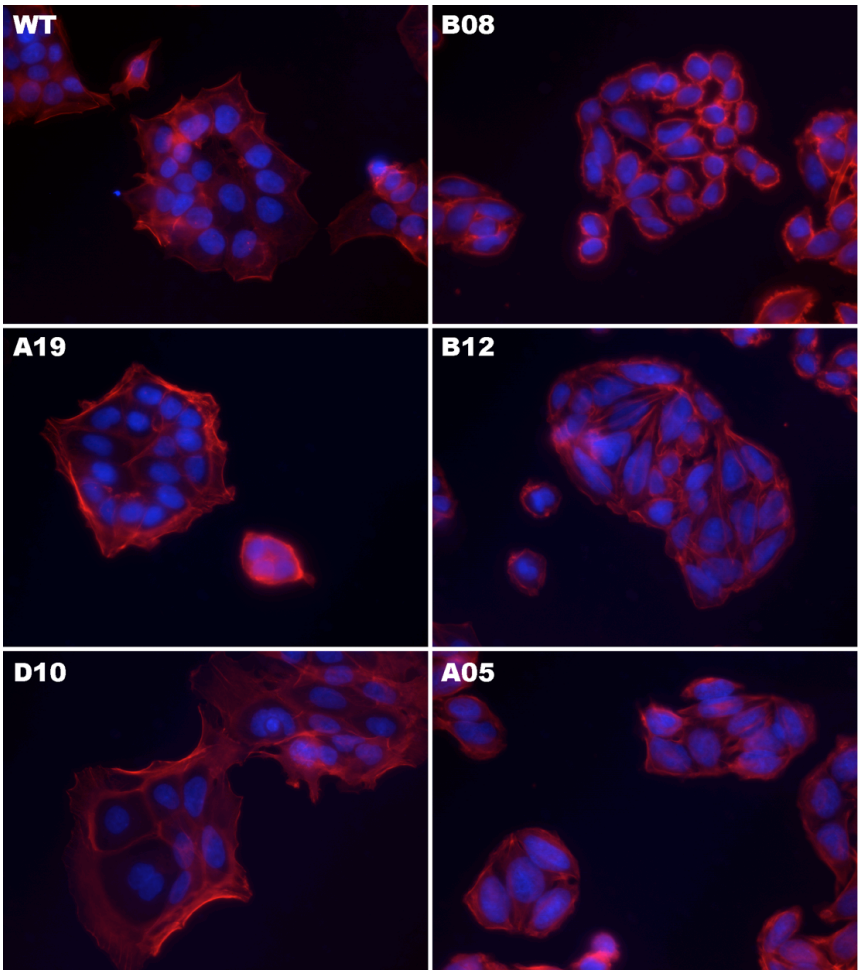

Figure 2.3 Immunofluorescence microscopy of wild-type (WT) HCT-8 cells and the five mutant cell lines.

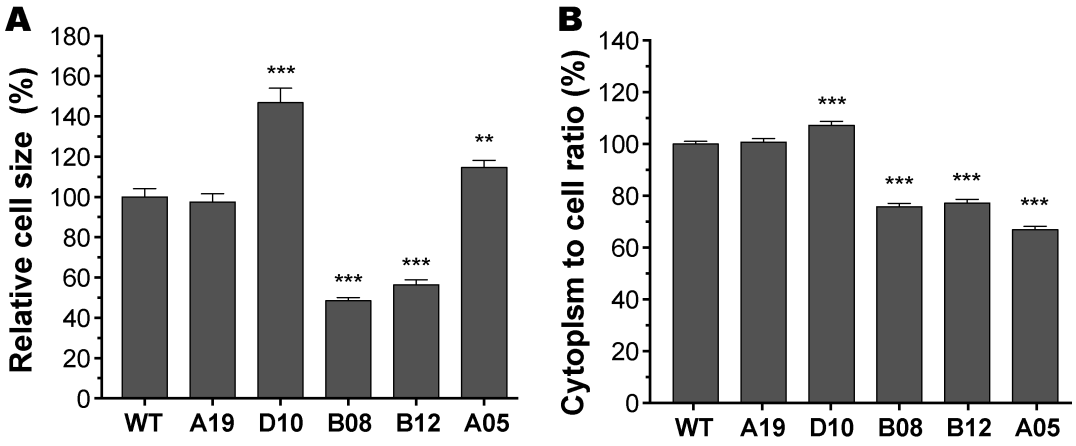

Figure 2.4 Size measurements of the cultured adherent cells from the six cell lines. (** = p <0.01; *** = p <0.001).

2.4 Conclusions

We have produced 43 mutated cell lines from the parent HCT-8 cells by UV-based mutagenesis, from which three mutants are significantly resistant to the *C. parvum* infection (i.e., A05, B08 and B12). Cell line A05 was found to be significantly resistant to the parasite attachment, while cell lines B08 and B12 were mainly resistant during *C. parvum* intracellular development. The three cell mutants may serve as valuable reagents to further study the mechanism of invasion and intracellular development by *C. parvum* by identifying the gene mutations associated with the phenotypic changes in the parasite attachment (i.e., A05) and intracellular development (i.e., B08 and B12).

CHAPTER III

INVOLVEMENT OF *Cryptosporidium parvum* ELONGATION FACTOR 1A (CPEF1A) IN THE HOST CELL F-ACTIN REORGANIZATION AND THE FORMATION OF PARASITOPHOROUS VACUOLE MEMBRANE (PVM)

3.1 Introduction

Cryptosporidium parvum is a globally distributed zoonotic apicomplexan parasite, and one of the major causative agents for cryptosporidiosis in humans and animals. In immunocompetent individuals, cryptosporidiosis causes mild to severe watery diarrhea, abdominal pain, vomiting, fever and weight loss (Bouzid et al. 2013). Children and individuals with a weakened or compromised immune system are at higher risk of severe infection. Studies have shown that cryptosporidiosis in children can lead to not only malnutrition, but also growth defects (Checkley et al. 2015, Chen et al. 2002).

Cryptosporidium parvum is transmitted by oocysts via the fecal-oral route, such as by drinking contaminated municipal or recreational waters (Prystajecky et al. 2014). When a human or animal host ingests oocysts, sporozoites are released from oocysts and invade intestinal epithelial cells. During the invasion, a sporozoite attaches onto the host cell surface, where the host cell membrane forms a fold to encircle the apical end of the zoite. The membrane fold/rim gradually rises up along the zoite and fuses together to fully cover the zoite (Valigurova et al. 2008). The process differs from other groups of apicomplexans that enter into the host cell cytosol (e.g., *Plasmodium, Toxoplasma* and *Eimeria*). In the meantime, the sporozoite undergoes a morphological change to become a round trophozoite during the invasion process, starting its intracellular, but extracytoplasmic development. The host cell-derived membrane containing the parasite is termed parasitophorous vacuole membrane (PVM), and is attached to the host cell by

a unique electron-dense (ED) structure layer padded by another F-actin-rich structure layer on the side of host cell. The remodeling of host cell F-actin is crucial for the formation of the actin filamentous network and PVM at an infection site (Elliott and Clark 2000).

The morphological changes of the parasites at the infection sites have been extensively studied, but the mechanisms involved in regulating the parasite attachment and invasion are poorly understood. A number of sporozoite surface proteins have been studied for their potential roles in attachment and invasion. These include parasite lectin-like proteins (e.g., p30 specific to Gal/GalNAc), mucin-like glycoproteins (e.g., gp40, gp45/15 and gp900), and thrombospondin-related adhesive proteins (TRAPs) (Hashim et al. 2006, Naitza et al. 1998, Petersen et al. 1992, Cevallos et al. 2000a, Cevallos et al. 2000b, Strong et al. 2000, Wanyiri et al. 2007b, O'Connor et al. 2007). Treatment by these proteins and/or their antibodies could reduce the parasite invasion and/or infection, implying their involvement in attachment and/or infection (Riggs et al. 2002). The circumsporozoite-like (CSL) protein is another glycoprotein that binds preferentially to epithelial cells, although the gene encoding CSL remains to be identified (Langer et al. 2001). Additionally, there are a number of other parasite surface proteins that could inhibit the parasite invasion at certain levels and/or possess immunodominant properties that imply their involvement in parasite-host cell interactions, such as *C. parvum* antigen 2 (CP2), antigen 47 (CP47), CPS-500, and Cpa135 (O'Hara et al. 2004, Nesterenko et al. 1999, Riggs et al. 1999, Riggs et al. 2002, Bonafonte et al. 2000, Perryman et al. 1996). Eukaryotic elongation Factor 1α (EF1α), the counterpart to the prokaryotic EF-Tu, is a family of highly conservative proteins that catalyze the binding of aminoacyl-tRNA to the ribosome (Lee et al. 1992, Li et al. 2013). In addition to the involvement in translational elongation, EF-Tu and EF1α are also known to participate in the modulation of cytoskeleton by interacting with the actin-like MreB protein in

prokaryotes and F-actin in eukaryotes (Defeu Soufo et al. 2010). We previously observed that the *CpEF1α* gene was highly expressed in the oocysts of *C. parvum* (i.e., top 5.5% among the 1924 expressed protein-encoding genes by microarray analysis) (Zhang et al. 2012b), followed by the confirmation of its high level of expression in sporozoites by qRT-PCR and by data-mining the proteomics datasets. The high abundance of CpEF1α in sporozoites prompted us to investigate its potential role as a structure protein in *C. parvum* and its involvement in the formation of the PVM and accumulation of host cell F-actin filaments during the parasite invasion and infection.

In the present study, we investigated the dynamic distribution of CpEF1α during parasite invasion and intracellular development, as well as the effect of CpEF1α, F-actin, and G-actin on the parasite invasion. The gene expression level of the CpEF1 family was also studied for different life stages of *C. parvum*. It is concluded that CpEF1α is involved in host cell actin filament reorganization and the formation of PVM during the parasite invasion.

3.2 Materials and Methods

3.2.1 Parasite material and in vitro cultivation

The oocysts of *C. parvum* (Iowa strain) were purchased from Bunch Grass Farm (Deary, ID) and stored in PBS containing penicillin (20 IU/mL) and streptomycin (20 μg/mL) at 4 °C. Before use, oocysts were purified by a Percoll gradient centrifugation, followed by treatment with 10% Clorox (~0.5% sodium hypochlorite) for 5 min on ice and 5-7 washes in phosphate-buffered saline (PBS; pH 7.4) by centrifugation (2,000 x g, 10 min each (Zhang et al. 2012b, Yu et al. 2017). After the final wash, oocysts were suspended in PBS, counted using a hemocytometer, and used immediately or stored at 4 °C. Free sporozoites were prepared by an in vitro excystation protocol, in which oocysts were incubated in PBS containing 0.25% trypsin and 0.5% taurodeoxycholic acid at 37 °C for 1 h, followed by 3-5 washes with PBS.

In vitro cultivation of *C. parvum* was hosted in a human ileocecal colorectal adenocarcinoma cell line (HCT-8; ATCC # CCL-224) as described (Arrowood 2002, Yu et al. 2017). Briefly, HCT-8 cells were seeded in 48-well cell culture plates or 24-well plates containing round glass coverslips in RPMI-1640 medium containing 10% fetal bovine serum (FBS) in an incubator with 5% CO_2 at 37 °C until they reached ~80% confluence or as specified. Oocysts or freshly prepared sporozoites were used to infect host cells for various times as specified in later sections. Oocysts less than 3 months old were used in all experiments. The viability of oocysts was also routinely examined by the in vitro excystation protocol to ensure that oocysts used in cultivation retained >80% excystation rate.

3.2.2 Cloning of CpEF1α gene and expression of recombinant protein

The *C. parvum* genome encodes a single copy of *CpEF1α* gene (GenBank: XM_001388307; CryptoDB gene ID: cgd6_3990). Because *CpEF1α* is an intronless gene, its open-reading frame (ORF) was amplified by PCR from the genomic DNA of *C. parvum* (IOWA strain from Bunch Grass Farm) using a high-fidelity *Pfu* DNA polymerase (Agilent Technologies, Inc. Santa Clara, CA) and a pair of primers CpEF1α-F-EcoRI (5′–tgaattcATGGGTAAGGAAAAGACTC–3′) and CpEF1α -R-PstI (5′–tctgcagCTTCTTCTTGGAAGTGGC–3′) (**Note**: Lower cases indicate added restriction linker sequences). The PCR product was cloned into a pCR4Blunt-TOPO vector (Invitrogen/Thermo Fisher Scientific, Grand Island, NY), followed by sequencing of plasmids to confirm the identity of inserts.

The *CpEF1α* ORF was then subcloned into a pMAL-c2E-TEV-His vector for expression as a maltose-binding protein (MBP) fusion protein. The expression vector was modified from pMAL-c2E vector (New England Biolabs) by adding a tobacco etch virus (TEV) protease

cleavage site between the MBP-tag and fused protein and a C-terminal His-tag (Wu et al. 2009). The resulting pMAL-CpEF1α plasmid was further verified by sequencing. The expression of recombinant MBP-CpEF1α protein was carried out in a Rossetta strain of *Escherichia coli* (Novagen). The expression and purification of CpEF1α using amylose resin-based affinity chromatography followed manufacturers' standard protocols as described previously (Guo and Zhu 2012, Zhang et al. 2015).

3.2.3 Expression of CpEF1α gene in various developmental stages of C. parvum

The relative levels of transcripts of *CpEF1α* and several elongation factor-related genes (i.e., *CpEF1β*, *CpEF1γ* and *CpERF3*) were evaluated by real-time quantitative RT-PCR (qRT-PCR) using a QIAGEN one-step RT-PCR QuantiTect SYBR green RT-PCR kit. The *C. parvum* lactate dehydrogenase (*CpLDH*) gene was also included as a reference (Zhang et al. 2015), and the parasite 18S rRNA (Cp18S) levels were used for normalization. Total RNA was isolated from *C. parvum* oocysts, free sporozoites, and intracellular stages using an RNeasy Mini kit (Qiagen, Inc., Valencia, CA). qRT-PCR reactions were performed in a CFX Connect real-time PCR detection system (Bio-Rad Laboratories, Hercules, CA), in which each reaction (10 μL) contained 0.6 ng of total RNA from oocysts or sporozoites, or 10 ng of total RNA from intracellular stages, 500 nM of primer for each specified gene (**Table 3.1**).

Table 3.1 List of primers used in this study

Gene Name		Sequence (5' – 3')
CpLDH (cgd7_480*)*	Forward	AAGCAAGGTCTTATCACCCAG
	Reverse	GCAAAGTAGGCAGTTCCTGTC
CpEF1α (cgd6_3990)	Forward	CTTCCGAAATGGGTAAGGG
	Reverse	TGGGGCATCAATGACAGTG
CpEF1 subunit α (cgd2_2070)	Forward	CTTGCGGATTAGTAGACCAGC
	Reverse	CCTCCCCACTTCCACAGTC
CpEF1β1 (cgd2_3950)	Forward	GCTATGGAAGCAAAGAAGAAGG
	Reverse	GCCACAGCATCTAAGTCAACATC
CpEF1γ (cgd7_4450)	Forward	CACGATTCTTGCTCAACCTTC
	Reverse	ATCCAGATTGGGGCTTAGC

To compare the relative levels of gene transcripts, we calculated the fluorescent units at cycle zero (F_0) for each gene transcript, including Cp18S, by a four-parametric sigmoidal curve fitting of the plots between the fluorescence readings (i.e., relative fluorescent unit; RFU) and thermal cycles using the following equation (Feng et al. 2008, Swillens et al. 2008, Rutledge 2004):

$$F_c = \frac{F_{max}}{1+e^{(C_{1/2}-C)/k}} + F_b \qquad (1)$$

where C was the cycle number, F_c was the RFU at cycle C, F_{max} was the maximum RFU, $C_{1/2}$ is the cycle when RFU reached to half of F_{max}, k was the slope of the sigmoid curve, and F_b was the background RFU. The Matlab code for calculating the F_0 values is deposited at GitHub (https://github.com/XueMaryYu/qRT-PCR-F0-calculation).

Because F_0 values were exact reflections of the initial target quantities expressed in fluorescence units, they could be directly used to compare the levels between different gene transcripts without prior knowledge of PCR amplification efficiencies (Rutledge 2004). In this study, the F_0 values of all gene transcripts were first normalized with those of Cp18S in individual samples.

The relative level of gene transcripts were then compared to the median value derived from the summation of genes in all samples.

3.2.4 Anti-CpEF1α antibody preparation and western blot analysis

Polyclonal anti-CpEF1α antibodies were prepared against a synthetic peptide specific to CpEF1α (^{156}CEYKQSRFDEIFNEVDGYLKK^{176}) in two specific pathogen-free (SPF) rabbits by a commercial custom antibody production service (Alpha Diagnostics International, San Antonio, TX). Antibodies were affinity-purified using agarose-resin conjugated with the synthetic peptide by Alpha Diagnostics International. The specificity of the polyclonal antibody was evaluated by Western blot analysis, in which *C. parvum* sporozoites prepared as described above were directly lyzed in a Laemmli sample buffer by 5 freeze-thaw cycles, followed by heating at 95 °C for 5 min, and finally centrifugation (10,000 × g, 5 min). Supernatants (representing ~1x10^7 sporozoites/lane) were subjected to 10% SDS-PAGE and transferred onto nitrocellulose membranes.

The nitrocellulose membranes were blocked by 5% nonfat milk in TBST buffer (Tris-buffered saline with 0.05% Tween-20, containing 150 mM NaCl, 50 mM Tris-HCl; pH 7.5) for 1 h. The blots were then incubated with affinity-purified rabbit anti-CpEF1α polyclonal antibody (1:500 dilution: ~0.8ng/mL) in 5% nonfat milk-TBST for 1 h, followed by 3 washes with TBST. Pre-immune rabbit serum (1:500 dilution) and the anti-CpEF1α antibody neutralized by pre-soaking it with recombinant CpEF1α protein (~0.5 μg/mL) were also used as controls. Next, the blots were treated with a horseradish peroxidase-conjugated goat anti-rabbit antibody in 5% nonfat milk-TBST for 1 h, followed by 3 washes with TBST. The blots were then visualized using enhanced chemiluminescence (ECL) on a HRP substrate (Sigma-Aldrich). All experimental procedures for Western blot analysis were conducted at room temperature.

3.2.5 Distributions of CpEF1α in sporozoites and in parasites during invasion and intracellular development, and co-localization with host cell F-actin

Various life cycle stages of *C. parvum,* including free sporozoites and intracellular parasites developed at various times, were prepared as described above. Free sporozoites after excystation were fixed with 4% paraformaldehyde in PBS for 20 min at room temperature, washed 3 times with PBS, suspended in water, and applied onto glass coverslips coated with poly-L-lysine. The coverslips were allowed to set for up to 1 h to permit sporozoites to settle onto the surface of the coverslips and for drying of the samples, followed by gentle washes with PBS.

For the preparation of sporozoites during the invasion, fresh free sporozoites (1×10^6/well) were incubated with HCT-8 cells grown on glass coverslips in 24-well plates for 35 min at 37 °C, followed by fixation with 4% paraformaldehyde in PBS for 20 min. Intracellular parasites developed after the invasion were prepared from oocysts incubated with HCT-8 cells cultured on coverslips for 3 h at 37 °C, followed by an exchange of culture medium to remove free parasites, and continued incubation. After continuous cultivation at 37 °C for a total 6 h, 10 h and 18 h, cell monolayers containing intracellular parasites were fixed with 4% paraformaldehyde in PBS for 20 min.

After fixation, all samples were washed with PBS and permeabilized with 0.1% Triton X-100 in PBS for 5 min. Samples were incubated with rhodamine-conjugated phalloidin (Thermo Fisher scientific; 1:500 dilution) for 45 min to stain host cell F-actin, followed by 3 washes with PBS. Slides were then incubated with affinity-purified anti-CpEF1α antibody or pre-immune serum at room temperature for 2 h, followed by incubation with a goat anti-rabbit IgG secondary antibody conjugated with fluorescein isothiocyanate (FITC). Coverslips were washed 3 times

with PBS after incubations with primary and secondary antibodies. Samples were mounted onto glass slides with Prolong Gold Antifade reagent containing 4', 6-diamidino-2-phenylindole (DAPI) to counter-stain nuclei (Molecular Probes/Invitrogen). Slides were examined with an Olympus BX51 research microscope equipped with a 100X/1.3 oil objective lens and appropriate filter sets for FITC and rhodamine, and/or with a Zeiss LSM 780 NLO multiphoton microscope equipped with a Plan-Apo 63X/1.46 oil objective lens. Fluorescent images were captured with a Retiga SRV CCD Digital Camera (QImaging, Olympus BX51) or a GaAsP NDD Detector for the Axio Examiner. All images were uniformly manipulated with Adobe Photoshop CS6 or CC for signal contrast and intensity. 3D images were generated with ZEN-2012 using images taken from a multiphoton microscope.

To illustrate the parasites and parasitophorous vacuole membranes (PVM) slides were stained with a rabbit polyclonal antibody against *C. parvum* total membrane proteins (CpTMPs), followed by incubation with the anti-CpTMP antibody at 1:400 dilution and goat anti-rabbit IgG antibody conjugated with tetramethylrhodamine isothiocyanate (TRITC) at concentrations recommended by manufacturers (Zhang and Zhu 2015, Chen et al. 2003, Zeng and Zhu 2006).

3.2.6 Evaluation of the effect of CpEF1α and related proteins on the parasite invasion

After observing the involvement of CpEF1α in the formation of the parasitophorous vacuole membrane (PVM) during invasion, we examined the effects of CpEF1α, F-actin, and G-actin on the parasite invasion and early stage of infection.

For the invasion assay, CpEF1α (100, 75, 50, 25 and 12.5 μg/mL), G-actin (50 μg/mL), F-actin (50 μg/mL), MBP (50 μg/mL), or combinations of CpEF1α with rabbit skeletal muscle G-actin or F-actin (50 μg/mL for each protein; Cytoskeleton, Inc.) were mixed with oocysts in serum-free culture medium containing BSA (50 μg/mL). BSA only (50 μg/mL) and MBP only

(50 μg/mL) were used as negative controls. After pre-incubation for 10 min, oocysts/protein suspensions were added to host cells cultured in 48-well plates at ~90% confluence at a rate of 5 × 10^4 oocysts/well. After incubation at 37 °C for 3 h to allow parasite excystation and invasion, uninfected parasites were removed by a medium exchange without proteins, followed by incubation for an additional 15 h at the same concentration (total 18 h infection time).

The cell culture plates were centrifuged for 5 min at 1,000 x g in a plate centrifuge (Heraeus Megafuge 16; Thermo Scientific, Waltham, MA) to ensure that all cells and potential free parasites in the medium were firmly attached to the bottom of the plates. The medium was removed and cells were gently rinsed with PBS twice, followed by centrifugation to remove residual PBS. Cells in each well were lysed using 200 μL of ice-cold Bio-Rad iScript qRT-PCR sample preparation reagent (iScript lysis buffer, Bio-Rad laboratories, Hercules, CA) after final centrifuging. Plates were shaken for 20 min using multi-tube verotexer at speed 7 (VX-2500, VWR International, Radnor, PA), followed by incubation at 80 °C for 15 min and centrifugation for 5 min at 1,000 x g. Supernatants were immediately used as RNA templates after dilution for qRT-PCR analysis or stored at -80 °C until use.

Parasite loads were evaluated by detecting the level of 18S rRNA transcripts from *C. parvum* (Cp18S) by qRT-PCR as described (Zhang and Zhu 2015). Briefly, cell lysates were diluted 40 fold using RNase/DNase-free water. Real-time qRT-PCR was performed using a CFX96 Touch Real-Time PCR Detection System (Bio-Rad Laboratories, Hercules, CA). Each well contained 4.5 μL of diluted cell lysate, 7.5 μL of One Step SYBR Green master mix, 0.15 μL of RT-master mix, 2.35 μL water, and 0.5 μL primer mix of Cp18S-1011F (5′-TTGTTC CTT ACT CCT TCA GCA C-3′) and Cp18S-1185R (5′-TCC TTC CTA TGT CTG GAC CTG-3′) (0.5 μM each) for Cp18S and Hs18S-1F (5’ GGC GCC CCC TCG ATG CTC TTA 3’) and

Hs18S-1R (5’ CCC CCG GCC GTC CCT CTT A 3’) for host cell 18S rRNA (Hs18S) (final volume 15 μL/well). The thermal cycles started with the synthesis of cDNA at 50 °C for 20 min, inactivation of reverse transcriptase at 95 °C for 5 min, and 40 cycles of PCR amplification, each at 95 °C for 10 sec and 58 °C for 30 sec. At least two technical replicates were performed for each sample using real-time qRT-PCR. Melting curves were analyzed between 65 °C and 95 °C at the end of PCR amplification. Amplification curves and melting peaks were examined to assess the quality and specificity of the reactions.

The computation of parasite loads based on the cycle threshold (C_T) values of Cp18S and Hs18S were similar as previously described (Zhang and Zhu 2015). In sum, the mean C_T value from technical replicates of each biological replicate were used to calculate C_T, the mean ΔC_T value between Cp18S and Hs18S were calculated by the equation ($\Delta C_T = C_{T[Cp18S]}-C_{T[Hs18S]}$), the mean $\Delta\Delta C_T$ value between each experimental sample and control were calculated by the equation ($\Delta\Delta C_T = \Delta C_{T[sample]}- \Delta C_{T[control]}$), and finally the relative level of gene expression was calculated using the empirical formula $2^{-\Delta\Delta C_T}$. The results were transformed to percentage $(100*2^{-\Delta\Delta C_T})\%$, and the statistical significance on the relative level of parasite 18S rRNA was evaluated by Student’s t-test.

To further validate the effect of CpEF1α on parasite invasion, we counted the number of invaded parasites after 3 h post infection under microscope. HCT-8 cells were cultured on glass coverslips in 24-well plates to ~90% confluence. Recombinant CpEF1α (MBP-tag or bovine serum albumin (BSA), each at 50 μg/mL) was pre-incubated with oocysts at 37 °C for 10 min, and the oocyst/protein suspensions were then added into individual wells (1×10^5 oocysts/well). After incubation at 37 °C for 3 h, wells were gently washed 3 times with PBS (10 min each) and fixed with 4% paraformaldehyde, followed by 3 washes with PBS (10 min each). Slides were

mounted with prolong gold anti-fade reagent with DAPI (Invitrogen), and the number of sporozoites counted with an Olympus BX51 research microscope under a 100X/1.3 oil objective lens. The experiments were repeated three times, each containing three biological replicates. For each biological replicate, 15 randomly selected microscopic fields were counted. The data was subjected to statistical analysis by a Student's *t*-test for significance between experiment and control groups (Yu et al. 2017).

3.3 Results

3.3.1 CpEF1α was one of the most highly expressed genes in oocysts and sporozoites of C. parvum *and up-regulated during the parasite infection*

In an earlier microarray-based transcriptomics analysis (Zhang et al. 2012b), we had noticed that *CpEF1α* was one of the most highly expressed genes in oocysts (i.e., # 106, or top 5.5%, among 1924 protein-coding genes (**Figure 3.1A**). We also datamined the published proteomics data available at the CryptoDB (http://cryptodb.org/cryptodb/) (Puiu et al. 2004), and observed that CpEF1α was ranked # 23 (top 2.1%) of the most abundant proteins in sporozoites (**Figure 3.1A**). For comparison, cgd2_2070 gene that encoded an EF1-related eukaryotic peptide chain release factor eRF3 (*CpeRF3*) was only ranked # 836 (top 43.6%) in oocyst transcriptomics and # 391 (34.9%) in sporozoite proteomics (**Figure 3.1A**). Note: cgd2_2070 was annotated as "translation elongation factor EF-1, subunit alpha, putative" by the CryptoDB because of the presence of the highly conserved EF1_alpha domain (cd01883 at the NCBI's Conserved Domain Database).

The high-level of expression of *CpEF1α* in oocysts and sporozoites was supported by qRT-PCR analysis, in which the *CpEF1α* transcript level in oocysts and sporozoites was 5 to 13-fold and 15 to 83-fold higher, respectively, than those of *CpEF1β*, *CpEF1γ* and *CpeRF3* (**Figure**

3.1B). The *CpEF1α* transcript levels were also much higher than those of *CpEF1β*, *CpEF1γ* and *CpeRF3* during intracellular developmental stages (i.e., 51 to 546-fold higher). While all EF1-related genes generally increased their expression levels during the development from oocysts to free sporozoites, and various intracellular stages, the evaluation of expression was much higher for *CpEF1α* than its related genes. *CpEF1α* showed a 60-fold increase when oocysts developed to sporozites, and a 133-fold increase when oocysts developed to intracellular stage at 6 h post infection time (vs. 16 to 47-fold for *CpEF1β*, 19 to 7-fold for *CpEF1γ* and 3.5 to 1.5-fold for *CpeRF3*, respectively) (**Figure 3.1B**).

A

Gene ID	Rank in oocysts by transcriptomics	Rank in sporozoite By proteomics
cgd6_3990 (CpEF1α)	106 (top 5.5%)	23 (top 2.1%)
cgd2_2070 (CpERF3)*	839 (top 43.6%)	391 (top 34.9%)

B

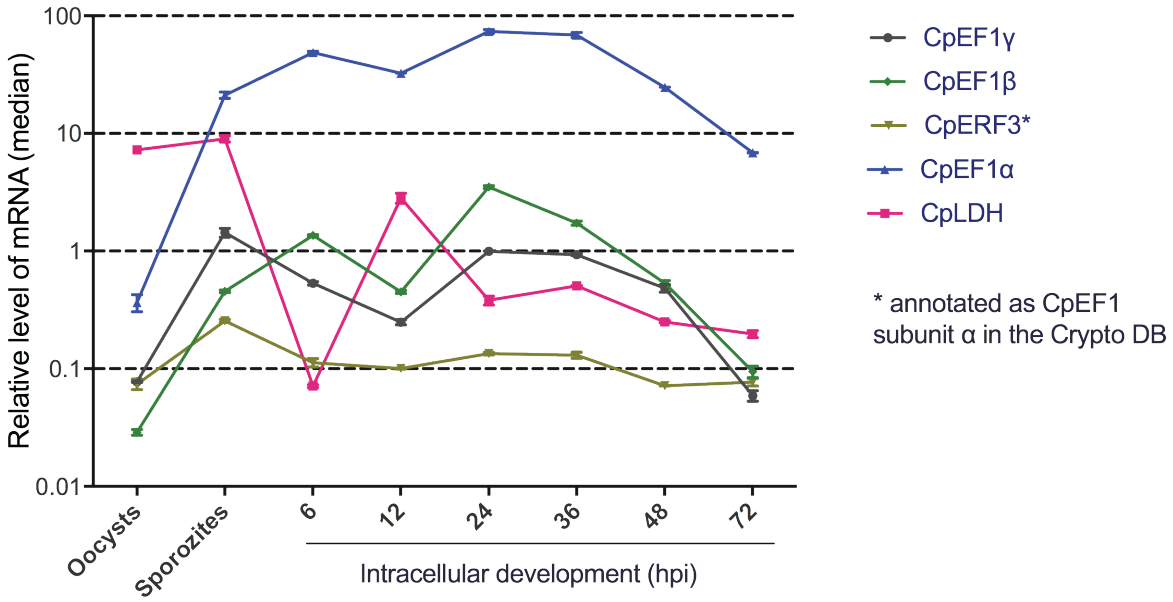

Figure 3.1 Comparison of *CpEF1α* gene expression and three other selected genes in the *CpEF1* gene family at different post-infection times.

As a reference, the expression profile of *CpLDH* gene differed from *CpEF1α* and other EF1-related genes, as *CpLDH* gene had it's highest expression in oocysts and sporozoites, which

agreed with previously reported data (Zhang et al. 2012b, Zhang et al. 2015), and confirmed the reliability of the expression profile data for *CpEF1α* and other EF1-related genes. Our observations were also supported by the transcriptomics data from Mauzy and colleagues (Mauzy et al. 2012), in which the expressions of *CpEF1α* and other EF1-related genes followed similar patterns (data not shown, but available at the CryptoDB).

3.3.2 CpEF1α protein distributed in the cytosol of sporozoites, trophozoites, and meronts

A rabbit polyclonal antibody against a CpEF1α-specific peptide was produced to investigate the distribution of CpEF1α protein in the parasite. Western blot analysis using this antibody detected single bands at ~47 kDa from whole proteins from sporozoites and ~90 kDa from recombinant CpEF1α with MBP-tag (**Figure 3.2A**). No immunoreactive bands were observed in the pre-immune serum or in the anti-CpEF1α antibody neutralized with CpEF1α protein. The broad band from recombinant CpEF1α was most likely signals derived from incompletely translated recombinant proteins. The sizes of the detected proteins agreed with the theoretical masses of native (~47 kDa) and the recombinant CpEF1α (~90 kDa) (**Figure 3.2B**), confirming the specificity of the antibody.

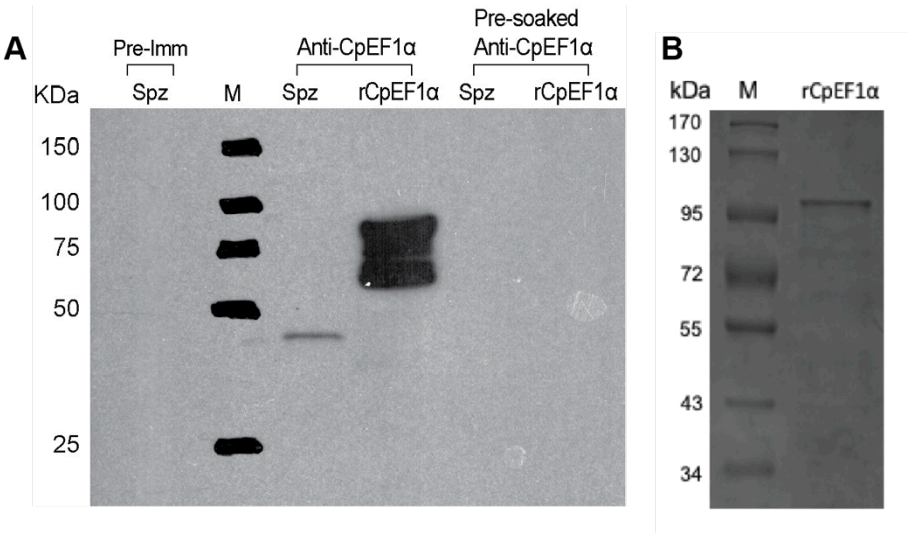

Figure 3.2 Western blot detection and protein expression of CpEF1α.

Immunofluorescence microscopy using this antibody revealed that CpEF1α was mostly distributed in the cytosol of free sporozoites, trophozoites with one nucleus, and meronts with 2 or more nuclei (**Figure 3.3**). No fluorescence signals were observed using rabbit pre-immune serum. The images of each column in Figure 3.3 are: (1) Differential interference microscopy (DIC); (2) nuclei counterstained with DAPI; (3) parasite CpEF1α labeled with FITC; (4) host F-actin stained with Rhodamine; (5) superimposed images of (2) – (4).

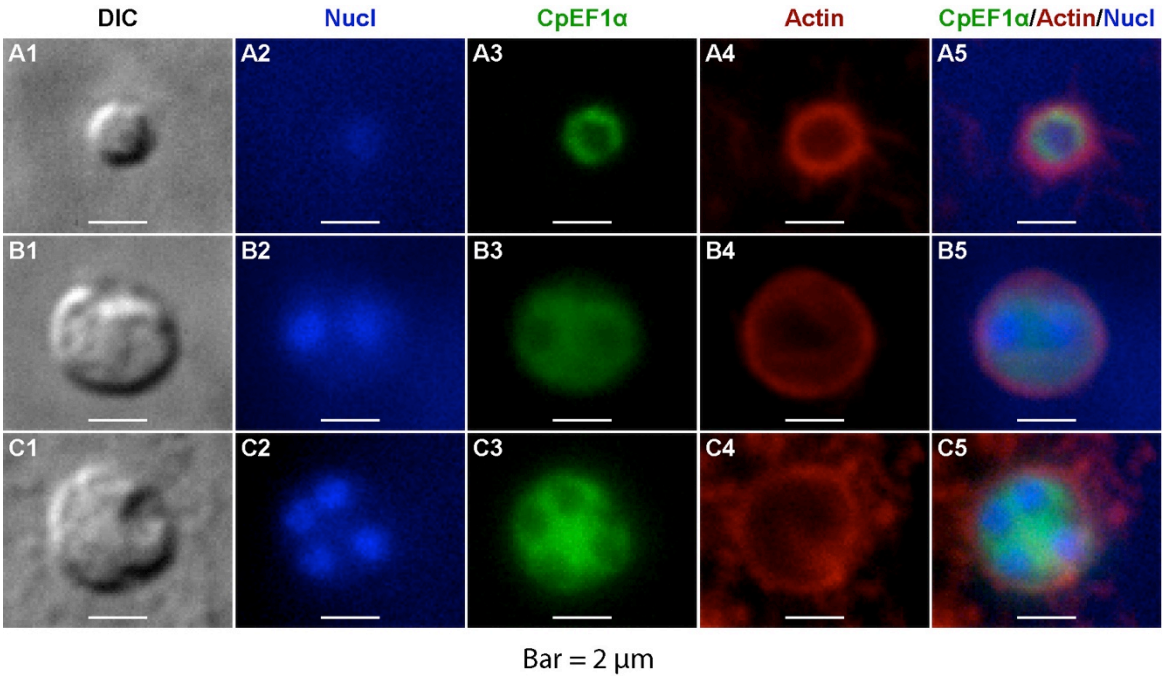

Figure 3.3 Detection of CpEF1α and host actin filaments intracellular stages by Immunofluorescence microscope.

There was evidence that some CpEF1α might be associated with the plasma membrane in the sporozoites (**Figure 3.4**). As seen in Figure 3.4, panel A1 is the DIC of normal sporozoites, panel A2 is the superimposed images of sporozoite CpEF1α and nucleus stain (CpEF1α/Nucl), panels B1and C1 are the DIC of damaged sporozoites, and panels B2 and C2 is the superimposed images of damaged sporozoite CpEF1α and nucleus stain, showing that some CpEF1α protein is associated with the plasma membrane. No or very weak signals were observed in the parasites and host cells incubated with pre-immune serum (Data not shown). By co-staining with phalloidin, we observed the accumulation of host cell F-actin at the infection site where the PVM started to form, which agreed with the observations by other investigators (Elliott and Clark 2000).

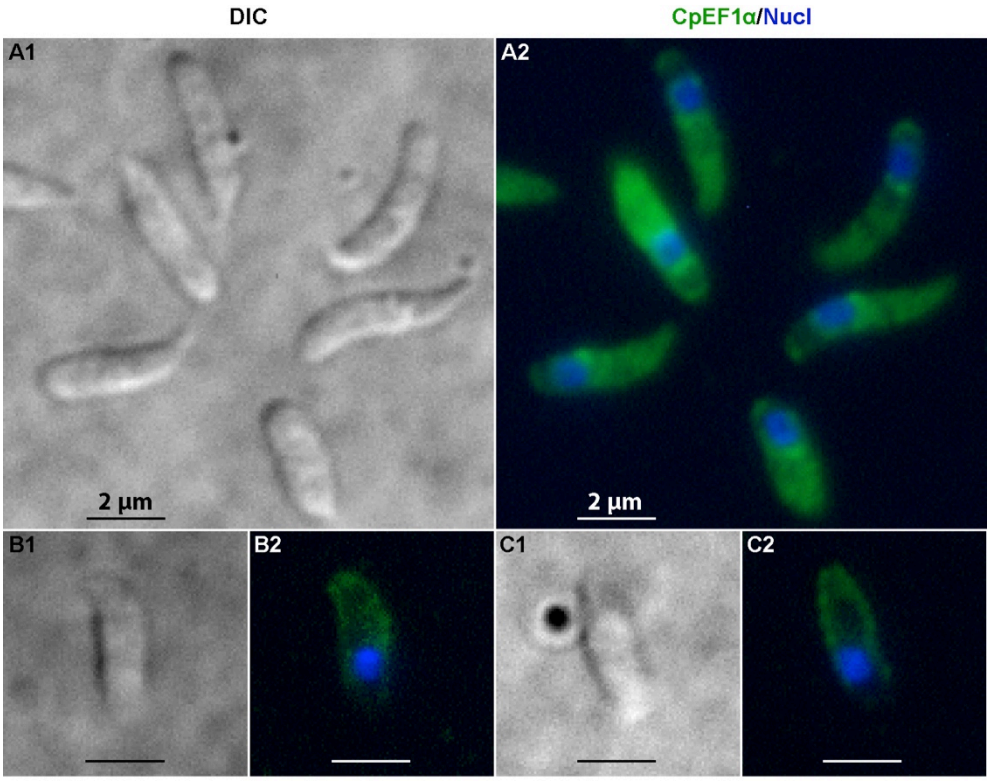

Figure 3.4 Detection of CpEF1α in normal sporozoites and damaged sporozoites by Immunofluorescence microscope.

3.3.3 CpEF1α was associated with the aggregation and extension of host cell F-actin during parasite invasion and PVM formation

The invasion of *C. parvum* sporozoites takes place in minutes, along with the engulfment of sporozoites by host cell plasma membrane to form PVM (Umemiya et al. 2005). The invasion is also accompanied by the shortening and transformation of sporozoites from a banana-like or rod-like shape to round-shaped trophozoites fully covered by the PVM (**Figure 3.5**). The movement of the host cell plasma membrane is generally driven by the rearrangements of actin filaments (Mogilner and Oster 1996, Lee and Dominguez 2010). We were motivated to test the potential role of CpEF1α in the formation of PVM during the parasite invasion due to the fact

that CpEF1α is highly abundant in sporozoites and that EF1α is capable of crosslinking actin filaments.

Immunofluorescence and multiphoton microscopic analyses revealed that, although abundant CpEF1α protein remained in sporozoites, a significant amount of CpEF1α protein was discharged onto the host cell plasma membrane at the infection site upon attachment of sporozoites onto host cells (**Figure 3.5; Figure 3.6**). The discharged CpEF1α formed a saucer or crescent shaped dense patch corresponding to the round dimple formed on the host cell surface at the invasion site. The stain of discharged CpEF1α maintained a saucer like shape throughout most of the the parasite invasion, but became weakened or dissolved after the PVM formation and transformation of sporozoites to trophozoites were complete, suggesting that discharged CpEF1α only coated the host cell membrane dimple, rather than penetrating into the host cell cytosol.

Intriguingly, the discharge of CpEF1α was clearly associated with the aggregation of host cell F-actin that formed a bulbous structure (i.e., Ø = ~0.5 μm globule) that was connected to, or partially overlapping with, the saucer shaped CpEF1α stain (**Figure 3.5; Figure 3.6**). During the process of sporozoite invasion, host cell actin filaments started to extend from the F-actin globule to surround sporozoites. In the meantime, the invading sporozoites underwent morphogenesis to form trophozoites, and became fully surrounded by host cell F-actin after trophozoites were fully formed, indicating the formation of intact PVM. These observations strongly suggested that, as an F-actin bundling protein, the discharged CpEF1α was involved in interacting with host cell F-actin to initiate the formation of the F-actin globule and the extension of actin filaments during the formation of PVM.

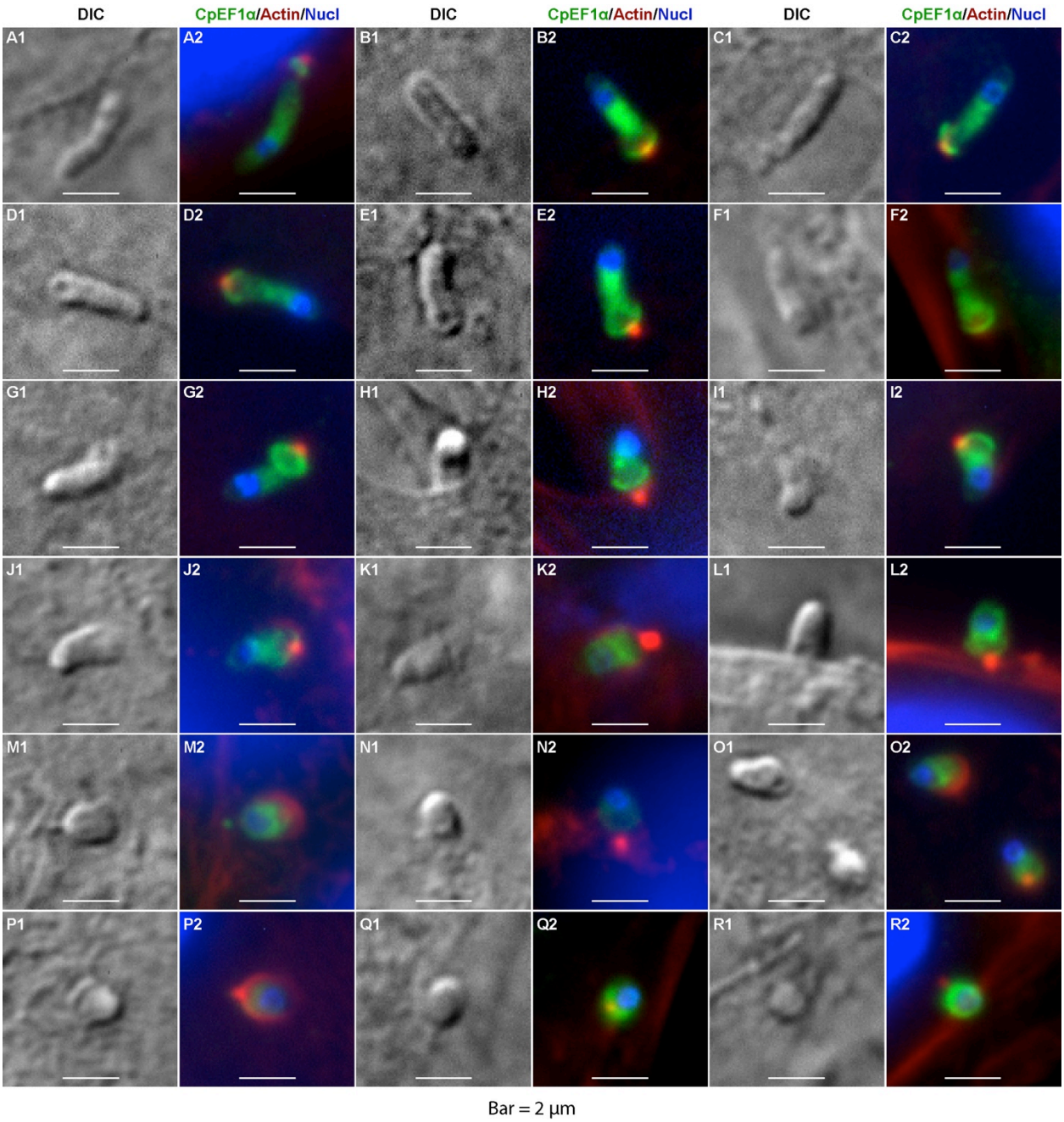

Figure 3.5 Detection of CpEF1α and F-actin distribution during parasite invasion by immunofluorescence microscope.

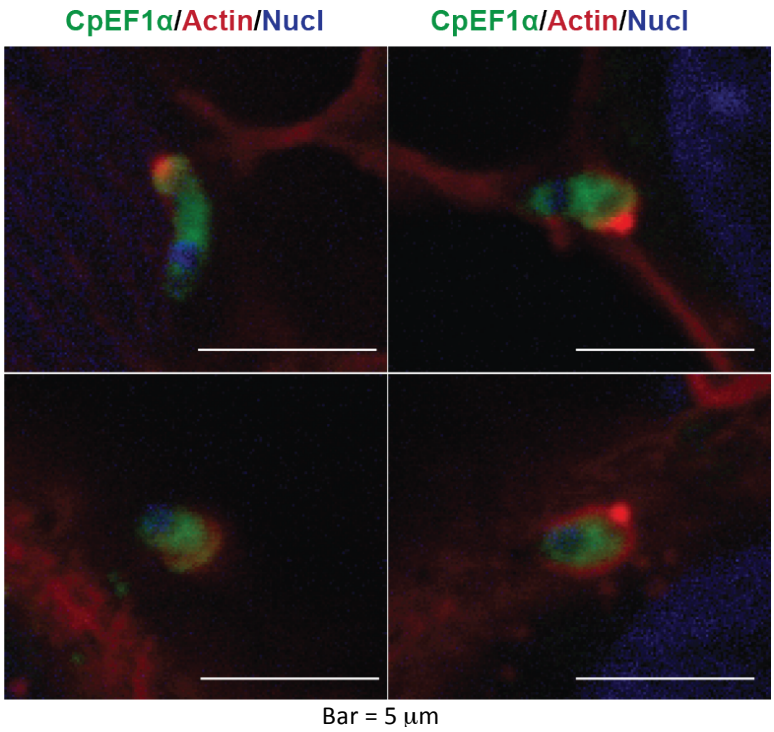

Figure 3.6 Detection of CpEF1α and F-actin distribution during parasite invasion multiphoton microscope.

3.3.4 Recombinant CpEF1α protein interfered with the invasion of C. parvum *sporozoites*

We further investigated the effects of CpEF1α and actin (50 μg/mL) on the *C. parvum* invasion, in which we observed that treatment with recombinant CpEF1α alone or in combination with G- or F-actin (each at 50 μM), but not G- or F-actin (50 μM) alone, could inhibit the parasite growth in an 18-h infection assay (e.g., by ~50% reduction of parasite load by qRT-PCR assay) (**Figure 3.7A**). In fact, the inhibition of parasite growth by recombinant CpEF1α was found to be dose-dependent, ranging from ~20 % inhibition at 12.5 μM to ~70 % inhibition at 100 μM (**Figure 3.7B**). We then confirmed that the inhibition of the parasite growth by CpEF1α was attributed to the reduction of invasion of sporozoites in a 3-h invasion assay (i.e., 59.5% reduction of invasion by microscopic counting the invaded sporozoites) (**Figure 3.8**).

The differential inhibitory effect of recombinant CpEF1α and G- or F-actin on the parasite invasion was likely due to the fact that CpEF1α is a highly charged protein (i.e., pI = 9.68). The charge of CpEF1α will make it easier for the protein adhere to the host cell surface, thus interfering with the subsequent action of CpEF1α discharged by sporozoites. On the other hand, actins are less charged (e.g., pI = ~6.0 for mammalian actins), so less actin proteins were present on the host cell surface to interfere with the action of discharged CpEF1α.

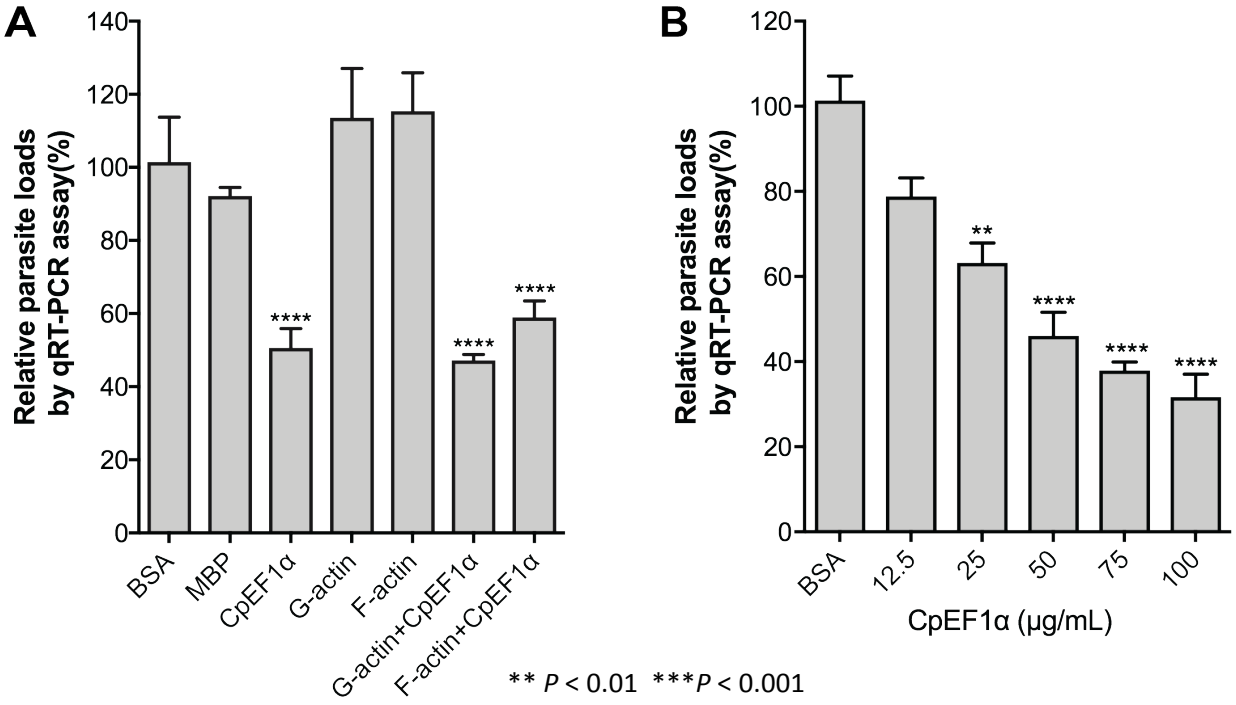

Figure 3.7 Effects of treatment by CpEF1α, F-actin, G-actin and their combinations on the invasion of *C. parvum* in HCT-8 cells.

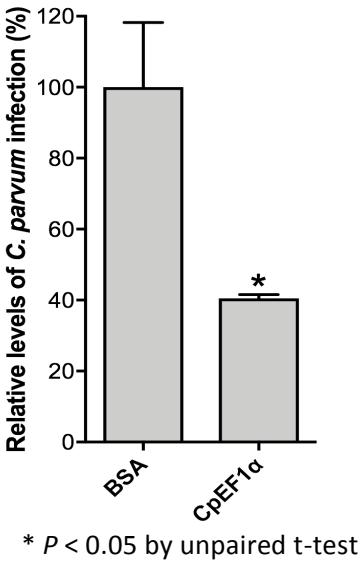

Figure 3.8 Effects of treatment by CpEF1α on the invasion of *C. parvum* in HCT-8 cells by microscopic counting.

3.4 Discussion

In the present study, we have confirmed that *CpEF1α* gene is expressed at much higher levels than other EF1-related genes at all developmental stages of in *C. parvum*. While CpEF1α is a cytosolic protein with some association to the plasma membrane in sporozoites, a significant amount of CpEF1α protein is discharged onto the host cell surface to form a saucer-shaped disc. We also observed the aggregation of host cell F-actin at the site of the discharged CpEF1α, from which F-actin extends to surround the invading sporozoites, corresponding to the formation of the PVM. Our data strongly indicates the involvement of CpEF1α with the host cell F-actin reorganization and the formation of the PVM during the parasite invasion. However, more direct evidence on the interaction of CpEF1α with host cell F-actin is needed to make firm conclusions, such as experiments to confirm the ability of CpEF1α to initiate the nucleation and aggregation of host cell actin filaments.

We have attempted multiple times to determine the subcellular locations of discharged CpEF1α and the F-actin globule by immuno-colloidal gold electron microscopy; however, we have failed each time when using the rabbit anti-CpEF1α polyclonal antibody for unknown reasons. We are currently generating new anti-CpEF1α antibodies and will undertake new experiments on protein subcellular localization.

The present study used phalloidin to label host cell F-actin. It is known that apicomplexan actin proteins might not be labeled by phalloidin, likely because actin protein is mostly present in globular form, or short filaments (Skillman et al. 2011, Skillman et al. 2013). We also confirmed that rhodamine-phalloidin staining was unable to produce any significant signals in *C. parvum* sporozoites (**Figure 3.9**), which confirms that rhodamine-phalloidin-stained actin filaments are truly derived from host cells; however, we could not rule out that parasite actin filaments might also be co-participated in the formation of PVM. It is also likely that *C. parvum* F-actin might interact with CpEF1α in the parasite. These notions can only be tested after the generation of new anti-*C. parvum* actin antibodies which is currently ongoing in our laboratory.

Nonetheless, our current data strongly implies the involvement of CpEF1α in the host cell F-actin reorganization and the formation of the PVM, which provides not only new knowledge on the functional role of CpEF1α in the parasite invasion into host cells, but also new insight into the poorly understood mechanism of the PVM formation.

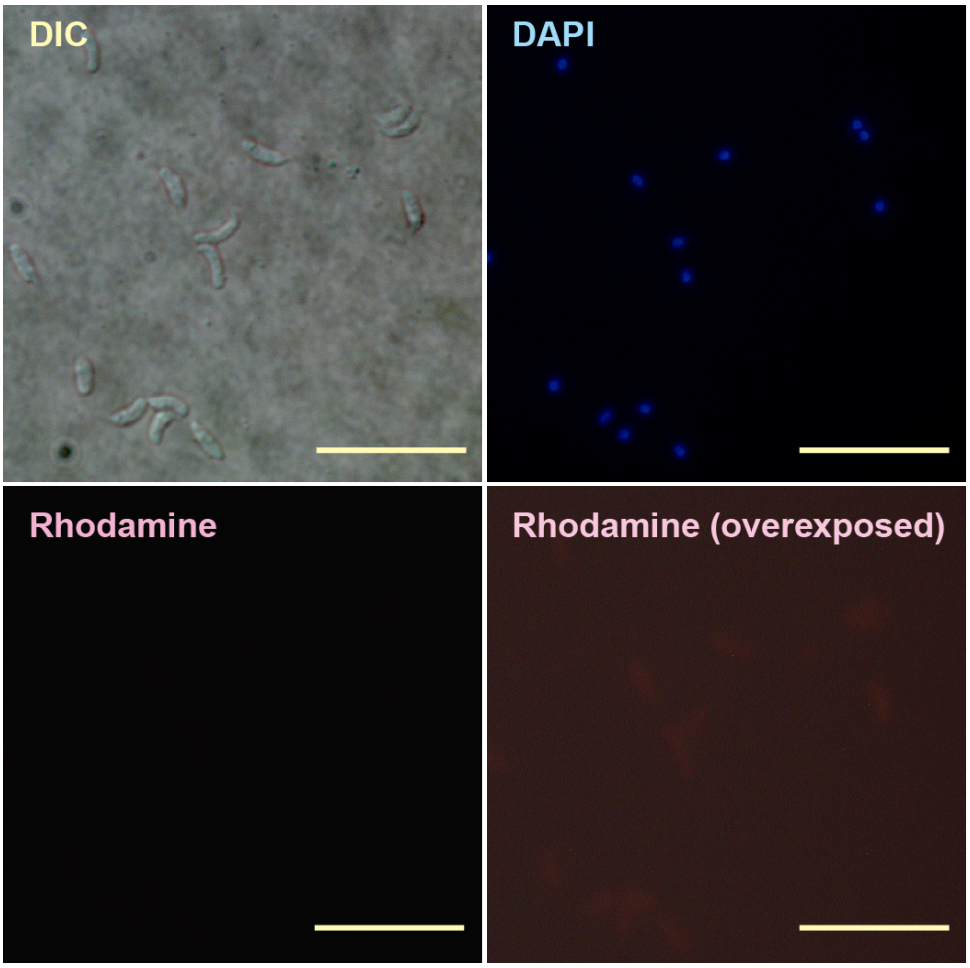

Figure 3.9 Rhodamine-phalloidin staining of the sporozoites actin.

CHAPTER IV

SUMMARY AND CONCLUSION

Cryptosporidium parvum is globally recognized as an important zoonotic pathogen causing mild to severe, or deadly, diarrheal diseases in humans and animals (Checkley et al. 2015, Ajjampur et al. 2010, Fletcher et al. 2012). This parasite infects intestinal epithelial cells in mammals to start its life cycle, for which the underlying molecular mechanisms are poorly understood. In the present study, we hypothesized that interactions between molecules from host cells and the parasite are critical to the establishment of *C. parvum* infection, and tested the hypothesis by focusing on the identification of host cell molecules associated with the parasite infection. A forward genetic approach was used to obtain host cell mutants by UV-irradiation of HCT-8 cells, cloning of irradiated host cells, and evaluation of cloned cells for their susceptibilities to infection by *C. parvum* in vitro. We produced 43 mutated cell lines from the parent HCT-8 cells, from which three mutant cell lines (A05, B08 and B12) were significantly resistant to *C. parvu*m infection and displayed decreased parasite load of approximately 50%, 30% and 20%, respectively. Cell line A05 was found to be significantly resistant to the *C. parvum* attachment, while cell lines B08 and B12 were mainly resistant during parasite intracellular development. Those three mutant cell lines can be used in subsequent analyses to identify genes and pathways associated with the phenotypic changes in the parasite attachment (i.e., A05) and intracellular development (i.e., B08 and B12).

In our preliminary studies, we observed that *CpEF1α* gene is highly expressed in the *C. parvum* sporozoites. We hypothesized that CpEF1α was involved in regulating the reorganization of host cell F-actin during invasion due to the fact that EF1α is also known as an

actin-binding protein, and that F-actin reorganization exists in the host cell at the *C. parvum* infection site. A set of experiments was performed to test this hypothesis. It was discovered through the use of immunofluorescence microscopy that CpEF1α protein was expressed throughout the parasite life cycle and was co-localized with host cell F-actin at the early stages of invasion. Incubation of CpEF1α protein (50 μg /mL) with oocysts for 3 h was found to reduce the parasite invasion by about 50% at 3 h and 18 h post infection times, indicating that CpEF1α was involved in the invasion process. The gene expression level of *CpEF1α* was much higher than the other genes in the *CpEF1* family, suggesting its importance for *C. parvum*. These observations indicate that CpEF1α plays an important role in *C. parvum* attachment and invasion process and may initiate host cell F-actin reorganization to start the parasite invasion process and participate in the parasite parasitophorous vacuole membrane (PVM) formation.

REFERENCES

Abrahamsen, M. S., Templeton, T. J., Enomoto, S., Abrahante, J. E., Zhu, G., Lancto, C. A., Deng, M., Liu, C., Widmer, G., Tzipori, S., Buck, G. A., Xu, P., Bankier, A. T., Dear, P. H., Konfortov, B. A., Spriggs, H. F., Iyer, L., Anantharaman, V., Aravind, L. & Kapur, V. 2004. Complete genome sequence of the apicomplexan, *Cryptosporidium parvum*. *Science,* **304:**441-5.

Abubakar, I., Aliyu, S. H., Arumugam, C., Usman, N. K. & Hunter, P. R. 2007. Treatment of cryptosporidiosis in immunocompromised individuals: systematic review and meta-analysis. *Br J Clin Pharmacol,* **63:**387-93.

Ajjampur, S. S., Liakath, F. B., Kannan, A., Rajendran, P., Sarkar, R., Moses, P. D., Simon, A., Agarwal, I., Mathew, A., O'Connor, R., Ward, H. & Kang, G. 2010. Multisite study of cryptosporidiosis in children with diarrhea in India. *J Clin Microbiol,* **48:**2075-81.

Amadi, B., Mwiya, M., Musuku, J., Watuka, A., Sianongo, S., Ayoub, A. & Kelly, P. 2002. Effect of nitazoxanide on morbidity and mortality in Zambian children with cryptosporidiosis: a randomised controlled trial. *Lancet,* **360:**1375-80.

Arrowood, M. J. 2002. In vitro cultivation of *Cryptosporidium* species. *Clin Microbiol Rev,* **15:**390-400.

Barnes, D. A., Bonnin, A., Huang, J. X., Gousset, L., Wu, J., Gut, J., Doyle, P., Dubremetz, J. F., Ward, H. & Petersen, C. 1998. A novel multi-domain mucin-like glycoprotein of *Cryptosporidium parvum* mediates invasion. *Mol Biochem Parasitol,* **96:**93-110.

Bhalchandra, S., Ludington, J., Coppens, I. & Ward, H. D. 2013. Identification and characterization of *Cryptosporidium parvum* Clec, a novel C-type lectin domain-containing mucin-like glycoprotein. *Infect Immun,* **81:**3356-65.

Bhat, N., Joe, A., PereiraPerrin, M. & Ward, H. D. 2007. *Cryptosporidium* p30, a galactose/N-acetylgalactosamine-specific lectin, mediates infection in vitro. *J Biol Chem,* **282:**34877-87.

Blackwell, J. L. & Brinton, M. A. 1997. Translation elongation factor-1 alpha interacts with the 3' stem-loop region of West Nile virus genomic RNA. *J Virol,* **71:**6433-44.

Bonafonte, M. T., Smith, L. M. & Mead, J. R. 2000. A 23-kDa recombinant antigen of *Cryptosporidium parvum* induces a cellular immune response on in vitro stimulated spleen and mesenteric lymph node cells from infected mice. *Exp Parasitol,* **96:**32-41.

Bonafonte, M. T., Priest, J. W., Garmon, D., Arrowood, M. J. & Mead, J. R. 1997. Isolation of the gene coding for elongation factor-1alpha in *Cryptosporidium parvum*. *Biochim Biophys Acta,* **1351:**256-60.

Borowski, H., Clode, P. L. & Thompson, R. C. 2008. Active invasion and/or encapsulation? A reappraisal of host-cell parasitism by *Cryptosporidium*. *Trends Parasitol,* **24:**509-16.

Bouzid, M., Hunter, P. R., Chalmers, R. M. & Tyler, K. M. 2013. *Cryptosporidium* pathogenicity and virulence. *Clin Microbiol Rev,* **26:**115-34.

Bunai, F., Ando, K., Ueno, H. & Numata, O. 2006. Tetrahymena eukaryotic translation elongation factor 1A (eEF1A) bundles filamentous actin through dimer formation. *J Biochem,* **140:**393-9.

Busch, D. B., Cleaver, J. E. & Glaser, D. A. 1980. Large-scale isolation of UV-sensitive clones of CHO cells. *Somatic Cell Genet,* **6:**407-18.

Bushkin, G. G., Motari, E., Carpentieri, A., Dubey, J. P., Costello, C. E., Robbins, P. W. & Samuelson, J. 2013. Evidence for a structural role for acid-fast lipids in oocyst walls of *Cryptosporidium*, *Toxoplasma*, and *Eimeria*. *MBio,* **4:**e00387-13.

Cai, X., Woods, K. M., Upton, S. J. & Zhu, G. 2005. Application of quantitative real-time reverse transcription-PCR in assessing drug efficacy against the intracellular pathogen *Cryptosporidium parvum* in vitro. *Antimicrob Agents Chemother,* **49:**4437-42.

Cevallos, A. M., Zhang, X., Waldor, M. K., Jaison, S., Zhou, X., Tzipori, S., Neutra, M. R. & Ward, H. D. 2000a. Molecular cloning and expression of a gene encoding *Cryptosporidium parvum* glycoproteins gp40 and gp15. *Infect Immun,* **68:**4108-16.

Cevallos, A. M., Bhat, N., Verdon, R., Hamer, D. H., Stein, B., Tzipori, S., Pereira, M. E., Keusch, G. T. & Ward, H. D. 2000b. Mediation of *Cryptosporidium parvum* infection in vitro by mucin-like glycoproteins defined by a neutralizing monoclonal antibody. *Infect Immun,* **68:**5167-75.

Checkley, W., White, A. C., Jr., Jaganath, D., Arrowood, M. J., Chalmers, R. M., Chen, X. M., Fayer, R., Griffiths, J. K., Guerrant, R. L., Hedstrom, L., Huston, C. D., Kotloff, K. L., Kang, G., Mead, J. R., Miller, M., Petri, W. A., Jr., Priest, J. W., Roos, D. S., Striepen, B., Thompson, R. C., Ward, H. D., Van Voorhis, W. A., Xiao, L., Zhu, G. & Houpt, E. R. 2015. A review of the global burden, novel diagnostics, therapeutics, and vaccine targets for *Cryptosporidium*. *Lancet Infect Dis,* **15:**85-94.

Chen, X. M. & LaRusso, N. F. 2000. Mechanisms of attachment and internalization of *Cryptosporidium parvum* to biliary and intestinal epithelial cells. *Gastroenterology,* **118:**368-79.

Chen, X. M., Keithly, J. S., Paya, C. V. & LaRusso, N. F. 2002. Cryptosporidiosis. *N Engl J Med,* **346:**1723-31.

Chen, X. M., Splinter, P. L., Tietz, P. S., Huang, B. Q., Billadeau, D. D. & LaRusso, N. F. 2004a. Phosphatidylinositol 3-kinase and frabin mediate *Cryptosporidium parvum* cellular invasion via activation of Cdc42. *J Biol Chem,* **279:**31671-8.

Chen, X. M., Huang, B. Q., Splinter, P. L., Cao, H., Zhu, G., McNiven, M. A. & LaRusso, N. F. 2003. *Cryptosporidium parvum* invasion of biliary epithelia requires host cell tyrosine phosphorylation of cortactin via c-Src. *Gastroenterology,* **125:**216-28.

Chen, X. M., Huang, B. Q., Splinter, P. L., Orth, J. D., Billadeau, D. D., McNiven, M. A. & LaRusso, N. F. 2004b. Cdc42 and the actin-related protein/neural Wiskott-Aldrich syndrome protein network mediate cellular invasion by *Cryptosporidium parvum*. *Infect Immun,* **72:**3011-21.

Chuang, S. M., Chen, L., Lambertson, D., Anand, M., Kinzy, T. G. & Madura, K. 2005. Proteasome-mediated degradation of cotranslationally damaged proteins involves translation elongation factor 1A. *Mol Cell Biol,* **25:**403-13.

Davis, W. G., Blackwell, J. L., Shi, P. Y. & Brinton, M. A. 2007. Interaction between the cellular protein eEF1A and the 3'-terminal stem-loop of West Nile virus genomic RNA facilitates viral minus-strand RNA synthesis. *J Virol,* **81:**10172-87.

Defeu Soufo, H. J., Reimold, C., Linne, U., Knust, T., Gescher, J. & Graumann, P. L. 2010. Bacterial translation elongation factor EF-Tu interacts and colocalizes with actin-like MreB protein. *Proc Natl Acad Sci U S A,* **107:**3163-8.

Demma, M., Warren, V., Hock, R., Dharmawardhane, S. & Condeelis, J. 1990. Isolation of an abundant 50,000-dalton actin filament bundling protein from Dictyostelium amoebae. *J Biol Chem,* **265:**2286-91.

Deng, M., Templeton, T. J., London, N. R., Bauer, C., Schroeder, A. A. & Abrahamsen, M. S. 2002. *Cryptosporidium parvum* Genes Containing Thrombospondin Type 1 Domains. *Infect Immun* , **70:**6987-6995.

Dunand, V. A., Hammer, S. M., Rossi, R., Poulin, M., Albrecht, M. A., Doweiko, J. P., DeGirolami, P. C., Coakley, E., Piessens, E. & Wanke, C. A. 1997. Parasitic sinusitis and otitis in patients infected with human immunodeficiency virus: report of five cases and review. *Clin Infect Dis,* **25:**267-72.

Duttaroy, A., Bourbeau, D., Wang, X. L. & Wang, E. 1998. Apoptosis rate can be accelerated or decelerated by overexpression or reduction of the level of elongation factor-1 alpha. *Exp Cell Res,* **238:**168-76.

Elitok, B., Elitok, O. M. & Pulat, H. 2005. Efficacy of azithromycin dihydrate in treatment of cryptosporidiosis in naturally infected dairy calves. *J Vet Intern Med,* **19:**590-3.

Elliott, D. A. & Clark, D. P. 2000. *Cryptosporidium parvum* induces host cell actin accumulation at the host-parasite interface. *Infect Immun,* **68:**2315-22.

Elliott, D. A., Coleman, D. J., Lane, M. A., May, R. C., Machesky, L. M. & Clark, D. P. 2001. *Cryptosporidium parvum* infection requires host cell actin polymerization. *Infect Immun,* **69:**5940-2.

Enriquez, F. J. & Riggs, M. W. 1998. Role of immunoglobulin A monoclonal antibodies against P23 in controlling murine *Cryptosporidium parvum* infection. *Infect Immun,* **66:**4469-73.

Fayer, R. & Leek, R. G. 1984. The effects of reducing conditions, medium, pH, temperature, and time on in vitro excystation of *Cryptosporidium*. *J Protozool,* **31:**567-9.

Feng, J., Zeng, R. & Chen, J. 2008. Accurate and efficient data processing for quantitative real-time PCR using a tripartite plant virus as a model. *Biotechniques,* **44:**901-12.

Fletcher, S. M., Stark, D., Harkness, J. & Ellis, J. 2012. Enteric protozoa in the developed world: a public health perspective. *Clin Microbiol Rev,* **25:**420-49.

Forney, J. R., Yang, S. & Healey, M. C. 1996. Protease activity associated with excystation of *Cryptosporidium parvum* oocysts. *J Parasitol,* **82:**889-92.

Forney, J. R., DeWald, D. B., Yang, S., Speer, C. A. & Healey, M. C. 1999. A role for host phosphoinositide 3-kinase and cytoskeletal remodeling during *Cryptosporidium parvum* infection. *Infect Immun,* **67:**844-52.

French, A. L., Beaudet, L. M., Benator, D. A., Levy, C. S., Kass, M. & Orenstein, J. M. 1995. Cholecystectomy in patients with AIDS: clinicopathologic correlations in 107 cases. *Clin Infect Dis,* **21:**852-8.

Fritzler, J. M. & Zhu, G. 2012. Novel anti-*Cryptosporidium* activity of known drugs identified by high-throughput screening against parasite fatty acyl-CoA binding protein (ACBP). *J Antimicrob Chemother,* **67:**609-17.

Gonen, H., Smith, C. E., Siegel, N. R., Kahana, C., Merrick, W. C., Chakraburtty, K., Schwartz, A. L. & Ciechanover, A. 1994. Protein synthesis elongation factor EF-1 alpha is essential for ubiquitin-dependent degradation of certain N alpha-acetylated proteins and may be substituted for by the bacterial elongation factor EF-Tu. *Proc Natl Acad Sci U S A,* **91:**7648-52.

Gross, S. R. & Kinzy, T. G. 2007. Improper organization of the actin cytoskeleton affects protein synthesis at initiation. *Mol Cell Biol,* **27:**1974-89.

Grosshans, H., Hurt, E. & Simos, G. 2000. An aminoacylation-dependent nuclear tRNA export pathway in yeast. *Genes Dev,* **14:**830-40.

Guo, F. & Zhu, G. 2012. Presence and removal of a contaminating NADH oxidation activity in recombinant maltose-binding protein fusion proteins expressed in *Escherichia coli*. *Biotechniques,* **52:**247-53.

Hashim, A., Mulcahy, G., Bourke, B. & Clyne, M. 2006. Interaction of *Cryptosporidium hominis* and *Cryptosporidium parvum* with primary human and bovine intestinal cells. *Infect Immun,* **74:**99-107.

Hayes, E. B., Matte, T. D., O'Brien, T. R., McKinley, T. W., Logsdon, G. S., Rose, J. B., Ungar, B. L., Word, D. M., Pinsky, P. F., Cummings, M. L. & et al. 1989. Large community outbreak of cryptosporidiosis due to contamination of a filtered public water supply. *N Engl J Med,* **320:**1372-6.

Inomata, A., Murakoshi, F., Ishiwa, A., Takano, R., Takemae, H., Sugi, T., Cagayat Recuenco, F., Horimoto, T. & Kato, K. 2015. Heparin interacts with elongation factor 1alpha of *Cryptosporidium parvum* and inhibits invasion. *Sci Rep,* **5:**11599.

Joe, A., Verdon, R., Tzipori, S., Keusch, G. T. & Ward, H. D. 1998. Attachment of *Cryptosporidium parvum* sporozoites to human intestinal epithelial cells. *Infect Immun,* **66:**3429-32.

Joe, A., Hamer, D. H., Kelley, M. A., Pereira, M. E., Keusch, G. T., Tzipori, S. & Ward, H. D. 1994. Role of a Gal/GalNAc-specific sporozoite surface lectin in *Cryptosporidium parvum*-host cell interaction. *J Eukaryot Microbiol,* **41:**44S.

Johnson, E. H., Windsor, J. J., Muirhead, D. E., King, G. J. & Al-Busaidy, R. 2000. Confirmation of the prophylactic value of paromomycin in a natural outbreak of caprine cryptosporidiosis. *Vet Res Commun,* **24:**63-7.

Kang, J. M., Ju, H. L., Yu, J. R., Sohn, W. M. & Na, B. K. 2012. Cryptostatin, a chagasin-family cysteine protease inhibitor of *Cryptosporidium parvum*. *Parasitology,* **139:**1029-37.

Khacho, M., Mekhail, K., Pilon-Larose, K., Pause, A., Cote, J. & Lee, S. 2008. eEF1A is a novel component of the mammalian nuclear protein export machinery. *Mol Biol Cell,* **19:**5296-308.

Khalyfa, A., Bourbeau, D., Chen, E., Petroulakis, E., Pan, J., Xu, S. & Wang, E. 2001. Characterization of elongation factor-1A (eEF1A-1) and eEF1A-2/S1 protein expression in normal and wasted mice. *J Biol Chem,* **276:**22915-22.

Kim, S. & Coulombe, P. A. 2010. Emerging role for the cytoskeleton as an organizer and regulator of translation. *Nat Rev Mol Cell Biol,* **11:**75-81.

Kugel, J. F. & Goodrich, J. A. 2006. Beating the heat: A translation factor and an RNA mobilize the heat shock transcription factor HSF1. *Mol Cell,* **22:**153-4.

Lal, A., Cornish, L. M., Fearnley, E., Glass, K. & Kirk, M. 2015. Cryptosporidiosis: A Disease of Tropical and Remote Areas in Australia. *PLoS Negl Trop Dis,* **9:**e0004078.

Langer, R. C. & Riggs, M. W. 1999. *Cryptosporidium parvum* apical complex glycoprotein CSL contains a sporozoite ligand for intestinal epithelial cells. *Infect Immun,* **67:**5282-91.

Langer, R. C., Schaefer, D. A. & Riggs, M. W. 2001. Characterization of an intestinal epithelial cell receptor recognized by the *Cryptosporidium parvum* sporozoite ligand CSL. *Infect Immun,* **69:**1661-70.

Lee, S., Francoeur, A. M., Liu, S. & Wang, E. 1992. Tissue-specific expression in mammalian brain, heart, and muscle of S1, a member of the elongation factor-1 alpha gene family. *J Biol Chem,* **267:**24064-8.

Lee, S. H. & Dominguez, R. 2010. Regulation of actin cytoskeleton dynamics in cells. *Mol Cells,* **29:**311-25.

Leitch, G. J. & He, Q. 2012. Cryptosporidiosis-an overview. *J Biomed Res,* **25:**1-16.

Lendner, M. & Daugschies, A. 2014. *Cryptosporidium* infections: molecular advances. *Parasitology,* **141:**1511-32.

Li, B., Wu, H., Li, N., Su, J., Jia, R., Jiang, J., Feng, Y. & Xiao, L. 2017. Preliminary Characterization of MEDLE-2, a Protein Potentially Involved in the Invasion of *Cryptosporidium parvum*. *Front Microbiol,* **8:**1647.

Li, D., Wei, T., Abbott, C. M. & Harrich, D. 2013. The unexpected roles of eukaryotic translation elongation factors in RNA virus replication and pathogenesis. *Microbiol Mol Biol Rev,* **77:**253-66.

Lidell, M. E., Moncada, D. M., Chadee, K. & Hansson, G. C. 2006. Entamoeba histolytica cysteine proteases cleave the MUC2 mucin in its C-terminal domain and dissolve the protective colonic mucus gel. *Proc Natl Acad Sci U S A,* **103:**9298-303.

Liu, G., Tang, J., Edmonds, B. T., Murray, J., Levin, S. & Condeelis, J. 1996. F-actin sequesters elongation factor 1alpha from interaction with aminoacyl-tRNA in a pH-dependent reaction. *J Cell Biol,* **135:**953-63.

Lumb, R., Smith, K., O'Donoghue, P. J. & Lanser, J. A. 1988. Ultrastructure of the attachment of *Cryptosporidium* sporozoites to tissue culture cells. *Parasitol Res,* **74:**531-6.

Ma, P. 1984. *Cryptosporidium* and the enteropathy of immune deficiency. *J Pediatr Gastroenterol Nutr,* **3:**488-90.

Ma, P. & Soave, R. 1983. Three-step stool examination for cryptosporidiosis in 10 homosexual men with protracted watery diarrhea. *J Infect Dis,* **147:**824-8.

Mac Kenzie, W. R., Hoxie, N. J., Proctor, M. E., Gradus, M. S., Blair, K. A., Peterson, D. E., Kazmierczak, J. J., Addiss, D. G., Fox, K. R., Rose, J. B. & et al. 1994. A massive outbreak in Milwaukee of *Cryptosporidium* infection transmitted through the public water supply. *N Engl J Med,* **331:**161-7.

Marcial, M. A. & Madara, J. L. 1986. *Cryptosporidium*: cellular localization, structural analysis of absorptive cell-parasite membrane-membrane interactions in guinea pigs, and suggestion of protozoan transport by M cells. *Gastroenterology,* **90:**583-94.

Marshall, R. J. & Flanigan, T. P. 1992. Paromomycin inhibits *Cryptosporidium* infection of a human enterocyte cell line. *J Infect Dis,* **165:**772-4.

Martin, K. C. & Ephrussi, A. 2009. mRNA localization: gene expression in the spatial dimension. *Cell,* **136:**719-30.

Matsubayashi, M., Teramoto-Kimata, I., Uni, S., Lillehoj, H. S., Matsuda, H., Furuya, M., Tani, H. & Sasai, K. 2013. Elongation factor-1alpha is a novel protein associated with host cell

invasion and a potential protective antigen of *Cryptosporidium parvum*. *J Biol Chem,* **288:**34111-20.

Matsuda, D., Yoshinari, S. & Dreher, T. W. 2004. eEF1A binding to aminoacylated viral RNA represses minus strand synthesis by TYMV RNA-dependent RNA polymerase. *Virology,* **321:**47-56.

Mauzy, M. J., Enomoto, S., Lancto, C. A., Abrahamsen, M. S. & Rutherford, M. S. 2012. The *Cryptosporidium parvum* transcriptome during in vitro development. *PLoS One,* **7:**e31715.

Meisel, J. L., Perera, D. R., Meligro, C. & Rubin, C. E. 1976. Overwhelming watery diarrhea associated with a *Cryptosporidium* in an immunosuppressed patient. *Gastroenterology,* **70:**1156-60.

Mogilner, A. & Oster, G. 1996. Cell motility driven by actin polymerization. *Biophys J,* **71:**3030-45.

Moncada, D., Keller, K. & Chadee, K. 2003. Entamoeba histolytica cysteine proteinases disrupt the polymeric structure of colonic mucin and alter its protective function. *Infect Immun,* **71:**838-44.

Morgan-Ryan, U. M., Fall, A., Ward, L. A., Hijjawi, N., Sulaiman, I., Fayer, R., Thompson, R. C., Olson, M., Lal, A. & Xiao, L. 2002. *Cryptosporidium hominis* n. sp. (Apicomplexa: Cryptosporidiidae) from *Homo sapiens*. *J Eukaryot Microbiol,* **49:**433-40.

Mullins, R. D., Heuser, J. A. & Pollard, T. D. 1998. The interaction of Arp2/3 complex with actin: nucleation, high affinity pointed end capping, and formation of branching networks of filaments. *Proc Natl Acad Sci U S A,* **95:**6181-6.

Murthi, A., Shaheen, H. H., Huang, H. Y., Preston, M. A., Lai, T. P., Phizicky, E. M. & Hopper, A. K. 2010. Regulation of tRNA bidirectional nuclear-cytoplasmic trafficking in *Saccharomyces cerevisiae*. *Mol Biol Cell,* **21:**639-49.

Na, B. K., Kang, J. M., Cheun, H. I., Cho, S. H., Moon, S. U., Kim, T. S. & Sohn, W. M. 2009. Cryptopain-1, a cysteine protease of *Cryptosporidium parvum*, does not require the pro-domain for folding. *Parasitology,* **136:**149-57.

Naitza, S., Spano, F., Robson, K. J. & Crisanti, A. 1998. The Thrombospondin-related Protein Family of Apicomplexan Parasites: The Gears of the Cell Invasion Machinery. *Parasitol Today,* **14:**479-84.

Nakamura, A. A. & Meireles, M. V. 2015. *Cryptosporidium* infections in birds--a review. *Rev Bras Parasitol Vet,* **24:**253-67.

Ndao, M., Nath-Chowdhury, M., Sajid, M., Marcus, V., Mashiyama, S. T., Sakanari, J., Chow, E., Mackey, Z., Land, K. M., Jacobson, M. P., Kalyanaraman, C., McKerrow, J. H., Arrowood, M. J. & Caffrey, C. R. 2013. A cysteine protease inhibitor rescues mice from a lethal *Cryptosporidium parvum* infection. *Antimicrob Agents Chemother,* **57:**6063-73.

Nelson, W. J. 2009. Remodeling epithelial cell organization: transitions between front-rear and apical-basal polarity. *Cold Spring Harb Perspect Biol,* **1:**a000513.

Nesterenko, M. V., Woods, K. & Upton, S. J. 1999. Receptor/ligand interactions between *Cryptosporidium parvum* and the surface of the host cell. *Biochim Biophys Acta,* **1454:**165-73.

Nime, F. A., Burek, J. D., Page, D. L., Holscher, M. A. & Yardley, J. H. 1976. Acute enterocolitis in a human being infected with the protozoan *Cryptosporidium*. *Gastroenterology,* **70:**592-8.

O'Connor, R. M., Wanyiri, J. W., Cevallos, A. M., Priest, J. W. & Ward, H. D. 2007. *Cryptosporidium parvum* glycoprotein gp40 localizes to the sporozoite surface by association with gp15. *Mol Biochem Parasitol,* **156:**80-3.

O'Connor, R. M., Burns, P. B., Ha-Ngoc, T., Scarpato, K., Khan, W., Kang, G. & Ward, H. 2009. Polymorphic mucin antigens CpMuc4 and CpMuc5 are integral to *Cryptosporidium parvum* infection in vitro. *Eukaryot Cell,* **8:**461-9.

O'Hara, S. P., Yu, J. R. & Lin, J. J. 2004. A novel *Cryptosporidium parvum* antigen, CP2, preferentially associates with membranous structures. *Parasitol Res,* **92:**317-27.

O'Connor, R. M., Wanyiri, J. W., Wojczyk, B. S., Kim, K. & Ward, H. 2007a. Stable expression of *Cryptosporidium parvum* glycoprotein gp40/15 in *Toxoplasma gondii*. *Mol Biochem Parasitol,* **152:**149-158.

Okhuysen, P. C., Chappell, C. L., Kettner, C. & Sterling, C. R. 1996. *Cryptosporidium parvum* metalloaminopeptidase inhibitors prevent in vitro excystation. *Antimicrob Agents Chemother,* **40:**2781-4.

Okhuysen, P. C., Rogers, G. A., Crisanti, A., Spano, F., Huang, D. B., Chappell, C. L. & Tzipori, S. 2004. Antibody response of healthy adults to recombinant thrombospondin-related

adhesive protein of *Cryptosporidium* 1 after experimental exposure to *Cryptosporidium* oocysts. *Clin Diagn Lab Immunol,* **11:**235-238.

Ollivett, T. L., Nydam, D. V., Bowman, D. D., Zambriski, J. A., Bellosa, M. L., Linden, T. C. & Divers, T. J. 2009. Effect of nitazoxanide on cryptosporidiosis in experimentally infected neonatal dairy calves. *J Dairy Sci,* **92:**1643-8.

Padda, R. S., Tsai, A., Chappell, C. L. & Okhuysen, P. C. 2002. Molecular cloning and analysis of the *Cryptosporidium parvum* aminopeptidase N gene. *Int J Parasitol,* **32:**187-97.

Perryman, L. E., Kapil, S. J., Jones, M. L. & Hunt, E. L. 1999. Protection of calves against cryptosporidiosis with immune bovine colostrum induced by a *Cryptosporidium parvum* recombinant protein. *Vaccine,* **17:**2142-9.

Perryman, L. E., Riggs, M. W., Mason, P. H. & Fayer, R. 1990. Kinetics of *Cryptosporidium parvum* sporozoite neutralization by monoclonal antibodies, immune bovine serum, and immune bovine colostrum. *Infect Immun,* **58:**257-9.

Perryman, L. E., Jasmer, D. P., Riggs, M. W., Bohnet, S. G., McGuire, T. C. & Arrowood, M. J. 1996. A cloned gene of *Cryptosporidium parvum* encodes neutralization-sensitive epitopes. *Mol Biochem Parasitol,* **80:**137-47.

Petersen, C., Gut, J., Doyle, P. S., Crabb, J. H., Nelson, R. G. & Leech, J. H. 1992. Characterization of a > 900,000-M(r) *Cryptosporidium parvum* sporozoite glycoprotein recognized by protective hyperimmune bovine colostral immunoglobulin. *Infect Immun,* **60:**5132-8.

Prystajecky, N., Huck, P. M., Schreier, H. & Isaac-Renton, J. L. 2014. Assessment of *Giardia* and *Cryptosporidium spp.* as a microbial source tracking tool for surface water: application in a mixed-use watershed. *Appl Environ Microbiol,* **80:**2328-36.

Puiu, D., Enomoto, S., Buck, G. A., Abrahamsen, M. S. & Kissinger, J. C. 2004. CryptoDB: the *Cryptosporidium* genome resource. *Nucleic Acids Res,* **32:**D329-31.

Ramirez, N. E., Ward, L. A. & Sreevatsan, S. 2004. A review of the biology and epidemiology of cryptosporidiosis in humans and animals. *Microbes Infect,* **6:**773-85.

Reduker, D. W. & Speer, C. A. 1985. Factors influencing excystation in *Cryptosporidium* oocysts from cattle. *J Parasitol,* **71:**112-5.

Richter, B., Nedorost, N., Maderner, A. & Weissenbock, H. 2011. Detection of *Cryptosporidium* species in feces or gastric contents from snakes and lizards as determined by polymerase

chain reaction analysis and partial sequencing of the 18S ribosomal RNA gene. *J Vet Diagn Invest,* **23:**430-5.

Riggs, M. W., McGuire, T. C., Mason, P. H. & Perryman, L. E. 1989. Neutralization-sensitive epitopes are exposed on the surface of infectious *Cryptosporidium parvum* sporozoites. *J Immunol,* **143:**1340-5.

Riggs, M. W., Cama, V. A., Leary, H. L., Jr. & Sterling, C. R. 1994. Bovine antibody against *Cryptosporidium parvum* elicits a circumsporozoite precipitate-like reaction and has immunotherapeutic effect against persistent cryptosporidiosis in SCID mice. *Infect Immun,* **62:**1927-39.

Riggs, M. W., Schaefer, D. A., Kapil, S. J., Barley-Maloney, L. & Perryman, L. E. 2002. Efficacy of monoclonal antibodies against defined antigens for passive immunotherapy of chronic gastrointestinal cryptosporidiosis. *Antimicrob Agents Chemother,* **46:**275-82.

Riggs, M. W., McNeil, M. R., Perryman, L. E., Stone, A. L., Scherman, M. S. & O'Connor, R. M. 1999. *Cryptosporidium parvum* sporozoite pellicle antigen recognized by a neutralizing monoclonal antibody is a beta-mannosylated glycolipid. *Infect Immun,* **67:**1317-22.

Rossignol, J. F., Ayoub, A. & Ayers, M. S. 2001. Treatment of diarrhea caused by *Cryptosporidium parvum*: a prospective randomized, double-blind, placebo-controlled study of Nitazoxanide. *J Infect Dis,* **184:**103-6.

Ruest, L. B., Marcotte, R. & Wang, E. 2002. Peptide elongation factor eEF1A-2/S1 expression in cultured differentiated myotubes and its protective effect against caspase-3-mediated apoptosis. *J Biol Chem,* **277:**5418-25.

Rutledge, R. G. 2004. Sigmoidal curve-fitting redefines quantitative real-time PCR with the prospective of developing automated high-throughput applications. *Nucleic Acids Res,* **32:**e178.

Schnyder, M., Kohler, L., Hemphill, A. & Deplazes, P. 2009. Prophylactic and therapeutic efficacy of nitazoxanide against *Cryptosporidium parvum* in experimentally challenged neonatal calves. *Vet Parasitol,* **160:**149-54.

Shahiduzzaman, M. & Daugschies, A. 2012. Therapy and prevention of cryptosporidiosis in animals. *Vet Parasitol,* **188:**203-14.

Shamovsky, I., Ivannikov, M., Kandel, E. S., Gershon, D. & Nudler, E. 2006. RNA-mediated response to heat shock in mammalian cells. *Nature,* **440:**556-60.

Skillman, K. M., Diraviyam, K., Khan, A., Tang, K., Sept, D. & Sibley, L. D. 2011. Evolutionarily divergent, unstable filamentous actin is essential for gliding motility in apicomplexan parasites. *PLoS Pathog,* **7:**e1002280.

Skillman, K. M., Ma, C. I., Fremont, D. H., Diraviyam, K., Cooper, J. A., Sept, D. & Sibley, L. D. 2013. The unusual dynamics of parasite actin result from isodesmic polymerization. *Nat Commun,* **4:**2285.

Smith, H. V., Nichols, R. A. & Grimason, A. M. 2005. *Cryptosporidium* excystation and invasion: getting to the guts of the matter. *Trends Parasitol,* **21:**133-42.

Spano, F., Puri, C., Ranucci, L., Putignani, L. & Crisanti, A. 1997. Cloning of the entire COWP gene of *Cryptosporidium parvum* and ultrastructural localization of the protein during sexual parasite development. *Parasitology,* **114 (Pt 5):**427-37.

Spano, F., Putignani, L., Naitza, S., Puri, C., Wright, S. & Crisanti, A. 1998. Molecular cloning and expression analysis of a *Cryptosporidium parvum* gene encoding a new member of the thrombospondin family. *Mol Biochem Parasitol,* **92:**147-62.

Stapulionis, R., Kolli, S. & Deutscher, M. P. 1997. Efficient mammalian protein synthesis requires an intact F-actin system. *J Biol Chem,* **272:**24980-6.

Strong, W. B., Gut, J. & Nelson, R. G. 2000. Cloning and sequence analysis of a highly polymorphic *Cryptosporidium parvum* gene encoding a 60-kilodalton glycoprotein and characterization of its 15- and 45-kilodalton zoite surface antigen products. *Infect Immun,* **68:**4117-34.

Swillens, S., Dessars, B. & Housni, H. E. 2008. Revisiting the sigmoidal curve fitting applied to quantitative real-time PCR data. *Anal Biochem,* **373:**370-6.

Takashima, Y., Xuan, X., Kimata, I., Iseki, M., Kodama, Y., Nagane, N., Nagasawa, H., Matsumoto, Y., Mikami, T. & Otsuka, H. 2003. Recombinant bovine herpesvirus-1 expressing p23 protein of *Cryptosporidium parvum* induces neutralizing antibodies in rabbits. *J Parasitol,* **89:**276-282.

Talapatra, S., Wagner, J. D. & Thompson, C. B. 2002. Elongation factor-1 alpha is a selective regulator of growth factor withdrawal and ER stress-induced apoptosis. *Cell Death Differ,* **9:**856-61.

Templeton, T. J., Lancto, C. A., Vigdorovich, V., Liu, C., London, N. R., Hadsall, K. Z. & Abrahamsen, M. S. 2004. The *Cryptosporidium* oocyst wall protein is a member of a multigene family and has a homolog in *Toxoplasma*. *Infect Immun,* **72:**980-7.

Theodos, C. M., Griffiths, J. K., D'Onfro, J., Fairfield, A. & Tzipori, S. 1998. Efficacy of nitazoxanide against *Cryptosporidium parvum* in cell culture and in animal models. *Antimicrob Agents Chemother,* **42:**1959-65.

Tosini, F., Agnoli, A., Mele, R., Gomez Morales, M. A. & Pozio, E. 2004. A new modular protein of *Cryptosporidium parvum*, with ricin B and LCCL domains, expressed in the sporozoite invasive stage. *Mol Biochem Parasitol* , **134:**137-147.

Travis, W. D., Schmidt, K., MacLowry, J. D., Masur, H., Condron, K. S. & Fojo, A. T. 1990. Respiratory cryptosporidiosis in a patient with malignant lymphoma. Report of a case and review of the literature. *Arch Pathol Lab Med,* **114:**519-22.

Tumwine, J. K., Kekitiinwa, A., Bakeera-Kitaka, S., Ndeezi, G., Downing, R., Feng, X., Akiyoshi, D. E. & Tzipori, S. 2005. Cryptosporidiosis and microsporidiosis in ugandan children with persistent diarrhea with and without concurrent infection with the human immunodeficiency virus. *Am J Trop Med Hyg,* **73:**921-5.

Tyzzer, E. E. 1907. A sporozoon found in the peptic glands of the common mouse. *Proc Soc Exp Biol Med,* **5:**12–13.

Tyzzer, E. E. 1910. An extracellular *Coccidium*, *Cryptosporidium Muris* (Gen. Et Sp. Nov.), of the gastric Glands of the Common Mouse. *J Med Res,* **23:**487-510 3.

Tyzzer, E. E. 1912. *Cryptosporidium parvum* (sp. nov.), a coccidium found in the small intestine of the common mouse. *Arch Protistenkd* **26:**394–412.

Tzipori, S., Smith, M., Birch, C., Barnes, G. & Bishop, R. 1983. Cryptosporidiosis in hospital patients with gastroenteritis. *Am J Trop Med Hyg,* **32:**931-4.

Tzipori, S., Campbell, I., Sherwood, D., Snodgrass, D. R. & Whitelaw, A. 1980. An outbreak of calf diarrhoea attributed to cryptosporidial infection. *Vet Rec,* **107:**579-80.

Tzipori, S. R., Campbell, I. & Angus, K. W. 1982. The therapeutic effect of 16 antimicrobial agents on *Cryptosporidium* infection in mice. *Aust J Exp Biol Med Sci,* **60:**187-90.

Umemiya, R., Fukuda, M., Fujisaki, K. & Matsui, T. 2005. Electron microscopic observation of the invasion process of *Cryptosporidium parvum* in severe combined immunodeficiency mice. *J Parasitol,* **91:**1034-9.

Valigurova, A., Jirku, M., Koudela, B., Gelnar, M., Modry, D. & Slapeta, J. 2008. Cryptosporidia: epicellular parasites embraced by the host cell membrane. *Int J Parasitol,* **38:**913-22.

Vera, M., Pani, B., Griffiths, L. A., Muchardt, C., Abbott, C. M., Singer, R. H. & Nudler, E. 2014. The translation elongation factor eEF1A1 couples transcription to translation during heat shock response. *Elife,* **3:**e03164.

Vetterling, J. M., Takeuchi, A. & Madden, P. A. 1971. Ultrastructure of *Cryptosporidium wrairi* from the guinea pig. *J Protozool,* **18:**248-60.

Wanyiri, J. W., O'Connor, R., Allison, G., Kim, K., , Kane, A., Qiu, J., Plaut, A. G. & Ward, H. D. 2007a. Proteolytic processing of the *Cryptosporidium* glycoprotein gp40/15 by human furin and by a parasite- derived furin-like protease activity. *Infect Immun,* **75:**184-192.

Wanyiri, J. W., O'Connor, R., Allison, G., Kim, K., Kane, A., Qiu, J., Plaut, A. G. & Ward, H. D. 2007b. Proteolytic processing of the *Cryptosporidium* glycoprotein gp40/15 by human furin and by a parasite-derived furin-like protease activity. *Infect Immun,* **75:**184-92.

Wu, X., Wu, D., Lu, Z., Chen, W., Hu, X. & Ding, Y. 2009. A novel method for high-level production of TEV protease by superfolder GFP tag. *J Biomed Biotechnol,* **2009:**591923.

Wyatt, C. R. & Perryman, L. E. 2000. Detection of mucosally delivered antibody to *Cryptosporidium parvum* p23 in infected calves. *Ann N Y Acad Sci,* **916:**378-87.

Wyatt, C. R., Brackett, E. J., Mason, P. H., Savidge, J. & Perryman, L. E. 2000. Excretion patterns of mucosally delivered antibodies to p23 in *Cryptosporidium parvum* infected calves. *Vet Immunol Immunopathol,* **76:**309-17.

Xiao, D., Yin, C., Zhang, Q., Li, J. H., Gong, P. T., Li, S. H., Zhang, G. C., Gao, Y. J. & Zhang, X. C. 2011. Selection and identification of a new adhesion protein of *Cryptosporidium parvum* from a cDNA library by ribosome display. *Exp Parasitol,* **129:**183-9.

Xu, P., Widmer, G., Wang, Y., Ozaki, L. S., Alves, J. M., Serrano, M. G., Puiu, D., Manque, P., Akiyoshi, D., Mackey, A. J., Pearson, W. R., Dear, P. H., Bankier, A. T., Peterson, D. L., Abrahamsen, M. S., Kapur, V., Tzipori, S. & Buck, G. A. 2004. The genome of *Cryptosporidium hominis*. *Nature,* **431:**1107-12.

Yamaji, Y., Sakurai, K., Hamada, K., Komatsu, K., Ozeki, J., Yoshida, A., Yoshii, A., Shimizu, T., Namba, S. & Hibi, T. 2010. Significance of eukaryotic translation elongation factor 1A in tobacco mosaic virus infection. *Arch Virol,* **155:**263-8.

Yang, F., Demma, M., Warren, V., Dharmawardhane, S. & Condeelis, J. 1990. Identification of an actin-binding protein from *Dictyostelium* as elongation factor 1a. *Nature,* **347:**494-6.

Yao, L., Yin, J., Zhang, X., Liu, Q., Li, J., Chen, L., Zhao, Y., Gong, P. & Liu, C. 2007. *Cryptosporidium parvum*: identification of a new surface adhesion protein on sporozoite and oocyst by screening of a phage-display cDNA library. *Exp Parasitol,* **115:**333-8.

Yu, Q., Li, J., Zhang, X., Gong, P., Zhang, G., Li, S. & Wang, H. 2010. Induction of immune responses in mice by a DNA vaccine encoding *Cryptosporidium parvum* Cp12 and Cp21 and its effect against homologous oocyst challenge. *Vet Parasitol,* **172:**1-7.

Yu, X., Zhang, H. & Zhu, G. 2017. Characterization of Host Cell Mutants Significantly Resistant to *Cryptosporidium parvum* Infection. *J Eukaryot Microbiol,* **64:**843-849.

Zeng, B. & Zhu, G. 2006. Two distinct oxysterol binding protein-related proteins in the parasitic protist *Cryptosporidium parvum* (Apicomplexa). *Biochem Biophys Res Commun,* **346:**591-99.

Zhang, H. & Zhu, G. 2015. Quantitative RT-PCR assay for high-throughput screening (HTS) of drugs against the growth of *Cryptosporidium parvum* in vitro. *Front Microbiol,* **6:**991.

Zhang, H., Guo, F. & Zhu, G. 2015. *Cryptosporidium* Lactate Dehydrogenase Is Associated with the Parasitophorous Vacuole Membrane and Is a Potential Target for Developing Therapeutics. *PLoS Pathog,* **11:**e1005250.

Zhang, H., Guo, F. & Zhu, G. 2012a. Involvement of host cell integrin alpha2 in *Cryptosporidium parvum* infection. *Infect Immun,* **80:**1753-8.

Zhang, H., Guo, F., Zhou, H. & Zhu, G. 2012b. Transcriptome analysis reveals unique metabolic features in the *Cryptosporidium parvum* Oocysts associated with environmental survival and stresses. *BMC Genomics,* **13:**647.